

Lawrence Berkeley National Laboratory

LBL Publications

Title

Permeation of CO₂ and N₂ through glassy poly(dimethyl phenylene) oxide under steady- and presteady-state conditions

Permalink

<https://escholarship.org/uc/item/0034p5sf>

Journal

Journal of Polymer Science, 58(9)

ISSN

2642-4150

Authors

Soniat, Marielle
Tesfaye, Meron
Mafi, Amirhossein
[et al.](#)

Publication Date

2020-05-01

DOI

10.1002/pol.20200053

Peer reviewed

1 Permeation of CO₂ and N₂ Through Glassy
2 Poly(Dimethyl Phenylene) Oxide (PPO)
3 under Steady and Pre-Steady State
4 Conditions

5 *Marielle Soniat*^{a,b}, *Meron Tesfaye*^{c,d}, *Amirhossein Mafi*^e, *Daniel J. Brooks*^e,
6 *Nicholas D. Humphrey*^e, *Lien-Chun Weng*^{a,d}, *Boris Merinov*^e, *William A.*
7 *Goddard, III*^e, *Adam Z. Weber*^{a,c}, and *Frances A. Houle*^{*,a,b}

8 a Joint Center for Artificial Photosynthesis, Lawrence Berkeley National
9 Laboratory, Berkeley, CA 94720, USA

10 b Chemical Sciences Division, Lawrence Berkeley National Laboratory,
11 Berkeley, CA 94720, USA

12 c Energy Storage and Distributed Resources Division, Lawrence Berkeley
13 National Laboratory, Berkeley, CA 94720, USA

14 d Department of Chemical and Biomolecular Engineering, University of
15 California, Berkeley, CA 94720, USA

16 e Materials and Process Simulation Center (MSC), Beckman Institute,
17 California Institute of Technology, Pasadena, CA 91125, USA

18 Abstract

19 Glassy polymers are often used for gas separations because of their high
20 selectivity. Although the dual mode permeation model correctly fits their
21 sorption and permeation isotherms, its physical interpretation is disputed,
22 and it does not describe permeation far from steady state, a condition
23 expected when separations involve intermittent renewable energy sources.
24 To develop a more comprehensive permeation model, we combine
25 experiment, molecular dynamics, and multiscale reaction-diffusion modeling
26 to characterize the time-dependent permeation of N₂ and CO₂ through a
27 glassy poly(dimethyl phenylene oxide) (PPO) membrane, a model system.
28 Simulations of experimental time-dependent permeation data for both gases
29 in the pre-steady state and steady state regimes show that both single-mode
30 and dual-mode reaction-diffusion models reproduce the experimental
31 observations, and that sorbed gas concentrations lag the external pressure
32 rise. The results point to environment-sensitive diffusion coefficients as a
33 vital characteristic of transport in glassy polymers.

34

35 Introduction

36 Non-porous polymeric materials are commonly used as membrane
37 separators for gas purification, reverse osmosis, and pervaporation, among
38 other applications.¹⁻⁵ For gas transport through any non-porous polymer, the
39 widely accepted model for permeability, P , is the solution-diffusion model,
40 which gives a phenomenological description of the permeability as the
41 product of the solubility coefficient, S , and the diffusion coefficient, D , at
42 steady state, i.e.,⁶⁻⁷

	$P = DS$	(1)
--	----------	-----

43 In the typical use of the solution-diffusion model, the diffusion coefficient is
44 assumed to be the proportionality constant between the flux and the
45 concentration (or chemical potential) gradient; as such, it should be constant
46 so long as the material properties and temperature are constant (Case I
47 diffusion).⁷⁻⁸ The diffusion rate may also depend on changes in the bulk
48 polymer morphology upon exposure to permeants (Case II diffusion) or a
49 combination of concentration gradient and polymer morphology change
50 (anomalous diffusion).⁸ In most studies, interactions between the polymer
51 and permeant causing, changes in polymer morphology over time (e.g.,
52 aging) and inhomogeneity in polymer morphology (e.g., different density in
53 the surface region) are not included explicitly using appropriate variables,
54 but instead are subsumed into the reported D .⁸⁻¹⁰ This limits the predictive
55 capabilities of the solution-diffusion model.

56 The standard application of the solution-diffusion model is as a steady-
57 state model, intended to describe situations where the membrane properties
58 and external conditions are constant. In cases where the polymer properties
59 change upon initial exposure to a permeant or where the external
60 permeation concentration is changing (e.g., produced in systems driven by
61 intermittent, renewable energy sources such as sunlight or wind^{4-5, 11-12}) such
62 non-steady state permeation cannot be predicted in a mechanistic way by
63 the solution-diffusion model. In contrast, physically-based, mechanistic
64 descriptions of permeation that capture time-dependent physical and
65 chemical processes will provide computational frameworks that are
66 predictive, afford greater scientific insight across length and timescales, and
67 apply to a wider range of permeation conditions. In previous studies,¹¹⁻¹² we
68 have reported such descriptions for gas sorption and permeation involving
69 rubbery polymer membranes and sorption of aqueous solutions of methanol
70 by Nafion. Those works allowed a multiscale simulation framework for
71 transport of weakly and strongly interacting permeants to be developed.
72 Although the systems studied are quite different chemically, the framework
73 has mechanistic elements common to both: interfacial transport, bulk
74 diffusion, and time-dependent solute concentrations. In this paper, we
75 extend the computational framework to represent permeation through
76 polymeric glasses, drawing on mechanisms proposed in the literature.¹³

77 A major difference between rubbery and glassy polymers is the
78 presence of excess fractional free volume (FFV) in the glassy state due to

79 kinetically trapped molecular chains.¹⁴⁻¹⁵ While FFV exists in all materials,¹⁶⁻¹⁸
 80 the excess FFV is proposed to play a special role in sorption and diffusion
 81 within glassy polymer materials.¹⁹ An increase in FFV has been shown to
 82 correlate with an increase in permeability and diffusion coefficients across a
 83 wide variety of glassy polymer compositions.²⁰ Positron annihilation lifetime
 84 spectroscopy (PALS) confirms that a discontinuity in the temperature
 85 dependence of the size of the void spaces, called free volume elements
 86 (FVE's), occurs at the same point as the discontinuity in the volume,¹⁸
 87 indicating that the excess FFV is mainly incorporated by increasing the size
 88 of the FVE's.²¹ The presence of excess FFV led to the proposal of the dual
 89 mode model, in which the total permeant solubility is given by two different
 90 modes within the polymer.¹³ The first mode is associated with sorption into
 91 the polymer matrix in the same manner as Henry's Law sorption into rubbers
 92 or liquids, and is often referred to as the dissolved mode. The second mode
 93 is associated with Langmuir-type adsorption to the internal surfaces of the
 94 FVEs, and has a non-linear relationship to the external pressure.¹⁹ The
 95 equation for the total pressure-dependent concentration of the gas, $[X](p)$,
 96 within a glassy polymer is

	$[X](p) = S_d p + \frac{S_L b_L}{1 + b_L p} p$	(2)
--	--	-----

97 where p is the external pressure, S_d is the dissolved solubility coefficient, and
 98 S_L is the Langmuir solubility coefficient, and b_L is the affinity parameter.¹⁹
 99 Commonly, separate diffusion coefficients are associated with each mode on

100 the basis of the dual mobility partial immobilization model,²²⁻²³ such that the
101 permeability isotherm²⁴ is given by

$P = S_d D_d + \frac{S_L b_L}{1 + b_L p_{up}} D_L$	(3)
--	-----

102 where D_d is the diffusion coefficient associated with dissolved sorption, and
103 D_L is the diffusion coefficient associated with Langmuir sorption. In total, five
104 fitting parameters are used to describe the observed decrease in
105 permeability and the decreasing effect on marginal sorption with increasing
106 pressure.^{19, 24} While the mathematical formulas for dual mode sorption fit the
107 isotherms well, the physical basis for this picture has been called into
108 question.²⁵⁻⁴⁰ For example, the amount of CO₂ absorbed into poly(dimethyl
109 phenylene oxide) (PPO) via the Langmuir mode is greater than that of N₂,⁴¹
110 even though N₂ has the smaller critical volume,¹⁶ defined as the volume
111 occupied by a molecule at the critical point in the phase diagram. The lesser
112 amount of N₂ sorbed into PPO contrasts with expectations from simple space-
113 filling arguments. Additionally, molecular dynamics (MD) simulations indicate
114 that voids are short-lived, and that diffusion in both rubbery and glassy
115 polymers is controlled by jumps between FVE;³⁵⁻³⁶ this indicates that the
116 contribution of the free volume to permeation may not be substantially
117 different from the rubbery case.

118 Herein, we investigate the applicability of modeling permeation
119 through glassy polymers with both single mode and dual mode models under
120 both non-steady state and steady state conditions. We investigate the
121 permeation of poly(dimethyl phenylene oxide) (PPO) by an inert gas, N₂, and

122 a plasticizing gas, CO₂. Physically based, multiscale simulations of time- and
123 pressure-dependent permeation data provide a sensitive test of a
124 permeation mechanism. Reaction-diffusion simulations, informed by
125 molecular dynamics calculations and experimental data, are performed for
126 comparison to experimental measurements made for this work. The results
127 show that models using either single or dual modes can describe gas
128 permeation through glassy PPO when the experimentally measured
129 pressure-dependent solubility and diffusion coefficients are used. However,
130 the time for the maximum gas uptake by the glassy polymer delayed relative
131 to the time for the upstream pressure rise, rather than being instantaneous
132 as in rubbery polymers.¹² The basic framework developed in this work will
133 serve as a foundation for the future study of permeation through polymer
134 electrolyte membranes (PEMs) formed from functionalized PPO that are
135 under development for solar fuels applications under steady-state and non-
136 steady state conditions.

137 Methods

138

139 1. Experimental

140 Complete time-dependent permeation data were measured for PPO as
141 a function of pressure for N₂ and CO₂. Materials preparation and
142 characterization, measurement methods, and data analysis are described in
143 this section. The permeation apparatus has been described previously.¹²

144 1A . Preparation of PPO Membranes

145 Powder poly(2,6-dimethyl-1,4-phenylene oxide) (PPO) was purchased
146 from Sigma Aldrich (St. Louis, MO) and dissolved in trichloroethane (ACS
147 Reagent, Sigma Aldrich) at a ratio of 10% by weight. The solution was stirred
148 continuously for 2 days and filtered with Millex PTFE filter (0.45 μ m, Millipore,
149 Burlington, MA) to ensure removal of undissolved powder lumps and
150 contaminants and to disperse large polymer aggregates that may have
151 formed. The solution was then degassed for about 20 minutes in a vacuum
152 desiccator to remove air bubbles formed during filtering process. The
153 manufacturer-provided PPO material characteristics are powder density of
154 1.06 g/cm³, glass transition temperature of 211 $^{\circ}$ C, and melting temperature
155 of 268 $^{\circ}$ C.

156 PPO samples were cast on silicon wafers in 3 layers in a class 100
157 clean room. Silicon wafers (6-inch, silicon 100, p-type, Pure Wafer, San Jose,
158 CA) were prepared by rinsing with deionized water, followed by blow drying
159 with N₂, two rinses with isopropyl alcohol, and finally drying with N₂. Each
160 wafer was placed on a hot plate at 373 K for 3-4 minutes to remove any
161 residual alcohol from the surface of the wafer. The first layer of PPO was cast
162 on a Silicon wafer and spun at 600 rpm for 200 s using a Laurell spin coater
163 (Laurell Technologies Corp., North Wales, PA). The layer was dried at room
164 temperature, then placed in a vacuum oven. Any trapped air pockets were
165 removed by switching the oven between a nitrogen purge and vacuum 3
166 times for 20-40 s each, and then drying under vacuum at 120 $^{\circ}$ C. The second
167 layer was cast on top of the first layer once it has cooled completely. The

168 same series of drying, purging, and vacuum drying were followed. The third
169 layer was formed in the same manner as the second layer. The drying times
170 for each layer are listed in Table 1. The final sample was cooled to room
171 temperature, cut into small pieces, and removed from the silicon wafer. Data
172 from 4 samples are reported in this work.

173

174 **Table 1.** Drying times after casting for each of the layers in the PPO sample.

Layer	Drying Time (min.)	
	Room Temperature	120°C in Vacuum
1	75	40
2	120	60
3	120	80

175

176 1B. Materials Characterization

177 The PPO film density was measured using helium gas pycnometer
178 (AccuPyc II 1340, Micromeritics, Norcross, GA). Films were cut into small
179 pieces and placed in sample cup (1 cm³ total) in the pycnometer. Each
180 sample was degassed 50 times to remove trapped air inside the cup, and the
181 occupied volume is measured with 30 repeats/sample. The measurement
182 was repeated 3 times. From the film density, the FFV was calculated using
183 the Bondi method.⁴²⁻⁴³

184 The glass transition temperature was measured using dynamic
185 scanning calorimetry (DSC 8000, Perkin Elmer, Waltham, MA). Samples were

186 placed in a DSC hermetic pan and subjected to a heating protocol of 3
187 heating steps followed by 2 cooling steps within the temperature window of
188 30-300°C at 20°C/min. The glass transition temperature was calculated from
189 the 2nd and 3rd heating step and averaged over 3 samples. Crystallinity, χ_c ,
190 was calculated using the melting onset and peak temperature.⁴⁴

191

192 1C. Permeation Measurements

193 PPO samples were placed in the permeation assembly, backed by a
194 filter paper, and sandwiched between two flat aluminum supports. The
195 aluminum supports allow for transport through a defined active area but do
196 not alter the measured permeability. The sample assembly was then placed
197 in the permeation cell for measurement.⁴⁵ All permeation experiments were
198 performed at 35°C. The sample was exposed to vacuum of 3 kPa or less for
199 at least 10 hrs to remove any residual water or gas pockets. Initially, the
200 downstream valve connecting the permeation cell to the vacuum pump was
201 closed, and any slow pressure rise in the downstream volume, $(dp_{ds}/dt)_{leak}$,
202 was monitored to test for leaks in the experimental apparatus. The sample
203 was then exposed to dry N₂ or CO₂ gas (99.995% pure, Praxair, Danbury, CT)
204 at the pressure of interest on the upstream side. Permeation through each of
205 the 4 samples was measured for both gases at all pressures. The upstream
206 pressure rise was recorded so that it can be included as part of the physical
207 system in the simulation. The system typically takes 2-25 s to reach its final
208 upstream pressure value, which ranges from 0-18 atm in this work. As gas
209 permeates through the membrane, the pressure rise in the closed

210 downstream volume, (dp_{ds}/dt) , was monitored. Once steady state was
 211 reached, signaled by a linear rise in downstream pressure over time,
 212 $(dp_{ds}/dt)_{SS}$, the permeability was calculated using the following equation,

$$P_m = \frac{Jl}{p_{up} - p_{ds}} = \frac{V_{ds}l}{\Delta p A R T} \left[\left(\frac{dp_{ds}}{dt} \right)_{SS} - \left(\frac{dp_{ds}}{dt} \right)_{leak} \right] \quad (4)$$

213 where P_m is the permeability of the membrane, J is the gas flux, l is the
 214 membrane thickness, Δp is the difference in upstream pressure, p_{up} , and
 215 downstream pressure, p_{ds} , A is the active area for flux measurements, V_{ds} is
 216 the downstream collection volume, R is the universal gas constant, and T is
 217 the temperature. This equation applies when $p_{up} \gg p_{ds}$ and p_{up} is constant;
 218 these conditions are met in our experiments during steady state. Values for l ,
 219 A , and V_{ds} are recorded in Table 2.

220

221 **Table 2.** Summary of experimental setup for each sample.

Sample	l	A	V_{ds}
	μm	cm^2	cm^3
1	32.25	0.970	41.73
2	22.42	0.495	41.73
3	19.39	0.495	41.73
4	19.39	0.495	41.73

222

223 1D. Calculation of Diffusion Coefficients

224 Sorption isotherms are fairly consistent across several literature
 225 studies of PPO,^{20, 24, 41, 46} and so we assume that our samples also have the

226 same solubility as that reported by Toi *et al.*,⁴¹ whose dual mode parameters
227 are reported in Table 3. Permeability and therefore diffusivity vary more
228 widely, and that is why we calculate the diffusion coefficients specific to our
229 samples of PPO. For reference, literature values of sorption and permeability
230 of CO₂ in PPO are reproduced in Supplementary Information (SI) Section 1.

231 Transport coefficients were calculated from the experimental data. In
232 the first method, the apparent diffusion coefficient, D_{app} , was calculated using
233 the standard single-mode solution-diffusion model (Eqn. 1). From the
234 experimental permeability and the apparent solubility, S_{app} , at a given
235 pressure p , the apparent diffusion coefficient, D_{app} , is given by

	$D_{app}(p) = \frac{P_m(p)}{S_{app}(p)}$	(5)
--	--	-----

236 where

	$S_{app}(p) = \frac{[X](p)}{p}$	(6)
--	---------------------------------	-----

237 In the second method, the experimental permeability versus upstream
238 pressure was fit to the dual mode model for permeation (Eqn. 3) with two
239 adjustable parameters D_H and D_L .

240 It is commonly reported that the diffusion coefficient can be calculated
241 independently from the lag time with the equation $\tau = l^2 / (6D)$, where τ is the
242 x-intercept in a plot of downstream quantity of gas vs. time. The time-lag
243 equation was derived with the assumption that the upstream pressure
244 increases from 0 to its steady-state value as a step function. In a real
245 experimental apparatus, however, the upstream pressure takes some time

246 to increase, and at early times, the downstream pressure vs. time data are
 247 dependent on the functional form and rate of the upstream pressure
 248 increase. When the lag time method was used to calculate D from our
 249 experimental data, 9% of the data had negative x-intercept, indicating a
 250 negative diffusion coefficient, clearly an unphysical result. Negative
 251 intercepts were especially common when the upstream pressure increase
 252 was slow and the sample permeance was high (high P_m , small l), such that
 253 the time for the pressure to rise and the time to reach steady state are
 254 comparable. Negative intercepts also occurred in our previous study on
 255 PDMS.¹² Modification of the time lag equation in the manner suggested by
 256 Paul and Koros²³ does not correct this issue. With the proper theoretical
 257 treatment, it should be possible to correct the time lag equation for a non-
 258 step function increase in upstream pressure, but such a treatment is beyond
 259 the scope of the current work.

260

261 **Table 3.** Solubility parameters for the dual mode model from Reference ⁴¹.

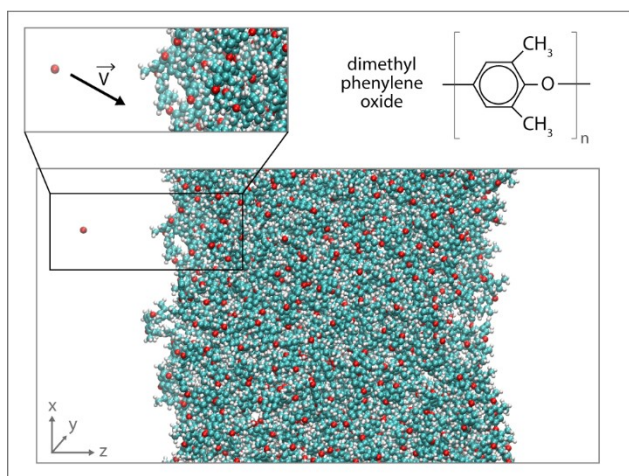
		N ₂	CO ₂
S_d	mol/(L atm)	5.28 × 10 ⁻³	4.18 × 10 ⁻²
S_L	mol/L	3.13 × 10 ⁻⁴	1.21 × 10 ⁻³
b_L	1/atm	0.040	0.25

262

263 2. Molecular Dynamics

264 One value that is essential to the multiscale model but unknown
265 experimentally is the sticking coefficient, which describes the probability of a
266 gas molecule impinging on the polymer surface sticking for long enough to
267 eventually be absorbed into the bulk polymer. To obtain this value, we
268 performed MD simulations of CO₂ colliding with PPO. An entangled polymer
269 structure consisting of 10 chains with 100 monomers per chain (17020
270 atoms) was created using the scaled effective solvent (SES) method⁴⁷ with
271 cell dimensions of 58.9 x 58.9 x 58.9 Å. To create a PPO surface, a surface-
272 cutting procedure was performed using the LAMMPS simulation package.⁴⁸
273 The length of the cell was increased by 200 Å in the z-direction to generate a
274 region of empty space. All polymer chains were kept intact. A virtual
275 Lennard-Jones wall was used to compact the dangling polymer chains at the
276 surface to produce a final thickness of 5.89 nm. The surface was then
277 equilibrated for 3000 ps in the NVT ensemble using the Berendsen
278 thermostat at 300 K with a damping constant of 0.1 ps. The OPLS-2005 force
279 field was used throughout.⁴⁹ The instantaneous surface was designated using
280 the Gaussian smoothing method of Willard and Chandler.⁵⁰ The final,
281 equilibrated structure has a density of 1.01 g/cm³ and is shown in Figure 1.

282



283

284 **Figure 1.** Polymer structure predicted from the molecular dynamics
 285 simulations, where blue represents carbon atoms, white is hydrogen, and red
 286 is oxygen. The molecule in the gas phase is CO₂, which is sent towards the
 287 surface with a velocity \vec{v} . The monomer 2,6-dimethyl-1,4-phenylene oxide
 288 chemical structure is shown on upper right.

289

290 A series of 265 simulations of CO₂ impacts onto the PPO surface was
 291 performed using the method from Julin *et al.*'s studies on the molecular
 292 adsorption.⁵¹⁻⁵² A CO₂ molecule was placed approximately 15 Å from the PPO
 293 surface and was sent toward the surface (z-component of the velocity within
 294 a 45-degree cone) with a speed chosen randomly from the Maxwell-
 295 Boltzmann distribution at 300 K. The surface region of PPO was defined as
 296 ± 4 Å of the instantaneous surface as defined by Willard and Chandler.⁵⁰ The
 297 position of the CO₂ molecule after 100 ps of NVE simulation determines the
 298 outcome - desorption, adsorption, or absorption. The impact simulations
 299 were performed using the Desmond MD simulation package⁵³⁻⁵⁵ with a time

300 step of 1.0 fs for short-range interactions and 3.0 fs for long-range
301 interactions. The short-ranged Coulomb cutoff is 9 Å and long-ranged
302 Coulomb interactions were computed using the Ewald summation. Further
303 details of the MD simulations can be found in our previous publication.¹²

304 Additionally, the free energy of CO₂ and N₂ within the polymer was
305 determined using molecular metadynamics simulations. Five gas molecules
306 were inserted into the simulation box, to produce a gas pressure of 2 atm;
307 when all 5 gas molecules are sorbed into the polymer, this produces a
308 concentration of 0.0404 mol/L. To estimate the free energy, one of the gas
309 molecules was biased to encourage it to explore all possible energetic states
310 through the thickness of the membrane while the other 4 gas molecules
311 were allowed to move freely through the gas phase and the polymer (i.e.
312 remain non-biased). The positions of 4 non-biased gas molecules were
313 averaged over ~750 ns for the CO₂-PPO system and 600 ns for the N₂-PPO
314 system to produce a number density, which gives an indication of the most
315 favorable position for those molecules within the polymer. The bias force was
316 directed from the center of mass of 1 gas molecule to and the center of mass
317 of the PPO slab, which was located approximately at the center of the box; a
318 counteracting force was applied to the polymer center of mass to prevent
319 drift. The bias force had a Gaussian width of 0.05 Å, an initial Gaussian
320 amplitude of 1.5 kJ/mol, a bias factor of 6, and a deposition period of 1.0 ps.
321 A virtual wall was placed on either side of the membrane at $z = \pm 5.2$ nm

322 with a force constant of 500 kJ/(mol nm²) in order to keep the gas molecules
323 near the membrane.

324 Calculations were performed with a time step of 1.0 fs in the NVT
325 ensemble using a stochastic global thermostat⁵⁶ with a coupling constant of
326 0.5 ps. The Lennard-Jones cut-off radius was 1.0 nm, where, the interaction
327 was smoothly shifted to 0 after 0.9 nm. Unlike-atom interactions were
328 computed using the standard Lorentz-Berthelot combination rules. Periodic
329 boundary conditions were applied to all three directions. The short-range
330 columbic interaction was treated within a cut-off radius of 1.0 nm while PME
331 algorithm⁵⁷ with a grid spacing of 0.16 nm was used to calculate the long-
332 range electrostatic interactions. All simulations were performed using
333 Gromacs-2016.4⁵⁸⁻⁵⁹ and plumed-2.4.1.⁶⁰ The OH-bonds on the PPO end
334 groups were constrained by P-LINCS algorithm⁶¹ with an order of 4. Further
335 details on the metadynamics simulations can be found in the SI Section 2.

336

337 3. Multi-Scale Simulations

338 3A. Inductive modeling approach

339 The permeation of small gaseous molecules through a PPO membrane
340 was simulated using multiscale reaction-diffusion kinetic models for single
341 mode and dual mode permeation. The approach in this style of modeling is
342 to assume the simplest description possible, then add complexity only when
343 necessary.⁶² For this reason, we begin with the model framework from a
344 study of permeation of gases through a rubbery polymer.¹² We then expand
345 upon that model by including dynamic changes in volume and the pressure-

346 dependent diffusion coefficients extracted from experiment. The goal of this
347 part of the study is to determine the simplest model based in fundamental
348 physical-chemical processes that reproduces the time-dependent permeation
349 data.

350 3B. Numerical Procedure

351 The reaction-diffusion scheme is solved using a stochastic method,⁶³⁻⁶⁴
352 a type of kinetic Monte Carlo (kMC), implemented in the open access
353 package Kinetiscope.⁶⁵ A detailed derivation of the basic simulation algorithm
354 for homogeneous, non-diffusing systems is given in Ref. ⁶⁴, and its extension
355 to simulate fully coupled reaction-diffusion systems is presented in Ref ⁶⁶.
356 Briefly, the reacting system is represented by a collection of particles, each
357 of which represents one or more molecules. All possible events in the system
358 are written as reaction (chemical or physical) or diffusion steps. The rates for
359 each reaction step are calculated in particles/sec units based on the rate
360 coefficient and current concentrations using their appropriate reaction
361 orders. The rates for each diffusion step are calculated based on the local
362 diffusion coefficient and the current concentration gradient, also in particles/
363 sec. All rates are converted to probabilities on a scale of 0 to 1 by dividing
364 each rate by the sum of all the rates. Events are selected among the
365 probability-weighted events using a random number between 0 and 1, and
366 the time step calculated using a second random number and the reciprocal
367 of the sum of the rates. After the event occurs and the simulation moves
368 forward in time, the concentrations and gradients are updated, and the

369 event selection cycle repeats. The simulation terminates when the
370 probability of all events falls to zero or a pre-specified time limit is reached.

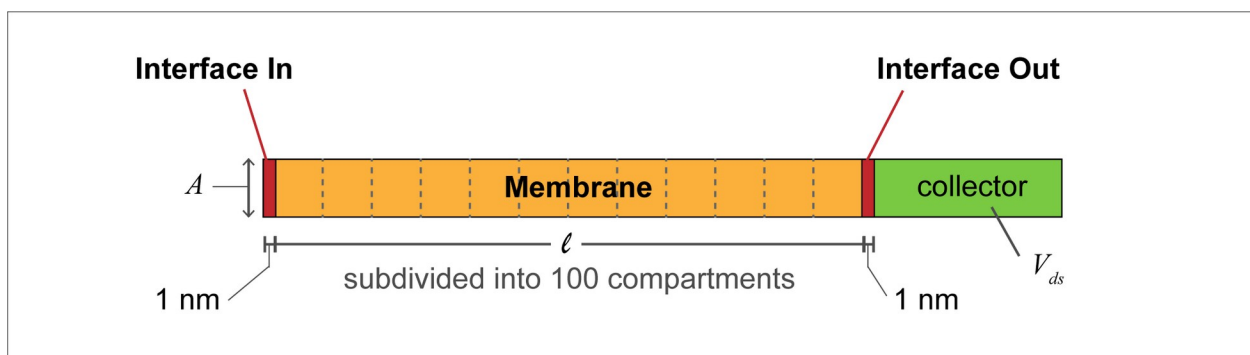
371 The stochastic method is a rigorous solution to the master equation for
372 Markov systems and produces an absolute time base when physically
373 meaningful rate coefficients are used, in contrast to other kMC methods that
374 only produce a relative time base. In addition, the stochastic method has
375 advantages over continuum methods since it provides for simulation of
376 complex systems in which swelling and other dynamic changes to the
377 reacting environment occur, and for which detail at both nano- and
378 macroscale dimensions is needed.

379

380 Model Development

381 The reaction-diffusion models are set up to allow for direct comparison
382 of simulation predictions to experimental data on downstream pressure rise,
383 as in our previous work.¹² A general schematic of the reaction-diffusion
384 system is shown in Figure 2.

385



386

387 **Figure 2.** Schematic of the multiscale reaction-diffusion system equivalent
388 to the membrane permeation system. The geometry, l , A , and V_{ds} , for each
389 sample is taken from the experimental setup in Table 2. The collector is
390 subdivided into 10 compartments with thicknesses increasing with distance
391 from the Interface Out plane. Adjacent compartments are connected by a
392 diffusion pathway for the gas.

393

394 1. Geometry

395 The cross-sectional area, A , upstream pressure, p_{up} , downstream
396 volume, V_{ds} , and initial membrane thickness, l , are set to experimental
397 values (see Table 2). The system is divided into a 1-dimensional array of
398 smaller compartments. The interfaces of the polymer with the gas phase are
399 assumed to be 1 nm thick on both sides of the membrane. The membrane
400 bulk is sub-divided into 100 compartments of equal thickness. The gas
401 collector with $V_{ds} = 41.73 \text{ cm}^3$ is divided into 10 compartments with gradually
402 increasing thickness starting from 10 nm and increasing in the direction
403 away from the downstream interface. This construct minimizes the number
404 of compartments required, and thus the cost of the simulation, while
405 preventing artificially high concentration gradients (and therefore fast
406 diffusion rates) that would have resulted if a large-volume collector
407 compartment were placed next to the thin interface compartment.

408 2. Interfaces

409 The adsorption and desorption physical reactions are shown in Scheme

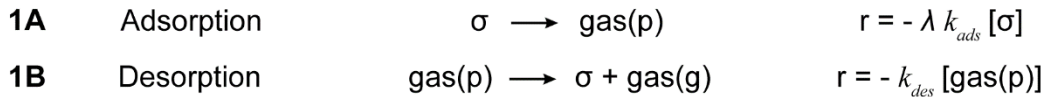
410 1. During adsorption, a site on the surface of the polymer, σ , accommodates

411 a gas molecule, which is denoted as gas(p), i.e. gas in the polymer phase.

412 Desorption is the reverse of this process.

413

Interface Reactions



414

415 **Scheme 1.** Reactions occurring in the interfacial compartments with their
416 associated rate laws. Adsorption takes place at Interface In, and desorption
417 at Interface Out. The reactant σ indicates a site on the surface of the
418 polymer. Reaction 1A is pseudo-first order in site concentration because the
419 upstream gas density is incorporated into k_{ads} (Equation 7).

420

421 The rate coefficient for interfacial adsorption, k_{ads} , is calculated from
422 gas kinetic theory for the collision frequency, Z , of a gas at a pressure p_{up}
423 with a planar surface at $T = 308$ K times the sticking probability, μ ,
424 determined from the molecular dynamics simulations.

$$k_{ads} = \mu Z A \lambda = \mu \left(\frac{p_{up}^{max}}{\sqrt{2\pi m k_B T}} \right) A \lambda \quad (7)$$

425 where m is the molecular mass of the gas, A is the surface area, and k_B is
426 Boltzmann's constant. The concentration of gas upstream is not included

427 explicitly in the rate equation for Reaction 1A because it is already included
428 in the k_{ads} via p_{up} . Because the upstream pressure does not instantly reach its
429 steady state value, the variable λ scales k_{ads} with the rise in upstream
430 pressure:

	$\lambda = \frac{p_{up}(t)}{p_{up}^{max}}$	(8)
--	--	-----

431 where $p_{up}(t)$ is the upstream pressure at time t , and p_{up}^{max} is the maximum
432 upstream pressure with which steady state properties are calculated.

433 During desorption, the gas in polymer moves to the gas phase in the
434 collector, denoted as gas(g), leaving behind an available surface site σ that
435 can be occupied by a new gas molecule emerging from the polymer bulk.
436 The desorption rate coefficient, $k_{des} = 1.4 \times 10^{11} \text{ s}^{-1}$, is calculated from the
437 Arrhenius equation using an activation energy for the breaking of a single
438 van der Waals bond in the gas phase, and the pre-exponential factor is
439 assumed to be 10^{13} .⁶⁷⁻⁶⁸

440 The concentration of surface sites is 1.66 mol/L, which is equal to a
441 liquid surface site density of $10^{14} \text{ atoms/cm}^2$,⁶⁹ distributed through the 1-nm
442 thickness of the interface. Our previous study¹² showed that the simulations
443 are insensitive to the surface site concentration so long as it is greater than
444 or equal to the bulk sorbed gas concentration.

445 3. Boundary Conditions and Diffusion Coefficients

446 Because we use a stochastic method, our boundary conditions (BC) are
447 implemented differently than in coupled differential equation (CDE) solvers.
448 Each compartment is connected to the adjacent compartments via Fickian

449 case I diffusion pathways for the sorbed gas molecules. Effects such as
450 swelling and polymer relaxation that would result in non-Fickian diffusion are
451 included explicitly as separate processes, and not integrated with the
452 diffusion coefficient (more details are provided below). The connection of
453 compartments by diffusion paths is analogous to flux (Neumann) BC in CDE,
454 with the flux dependent on the local, time-dependent concentrations. The
455 center-to-center distance between adjacent compartments is used for the
456 calculation of concentration gradients.

457 The diffusion coefficients for gases within the membrane are calculated
458 as described in Methods Section 2. Gases that have desorbed from the
459 membrane move into and within the downstream collector volume with
460 $D(\text{gas}(g)) = 7.43 \times 10^{-4} \text{ m}^2/\text{s}$, consistent with the mean free path and
461 average velocity of CO_2 in the gas phase.⁷⁰ Gas molecules only contribute to
462 p_{ds} once they are in the collector region, away from the membrane interface.
463 Additional details for the gas collector compartments are available in the SI
464 Section 3.

465 4. Initial Conditions and Pressure-Dependent Concentration of 466 Permeants

467 The simulation start time is set to the beginning of the rise in upstream
468 pressure, p_{up} , in the experiment, and the experimentally recorded $p_{up}(t)$ is
469 used as an input. In literature models, the concentration at the interface and
470 the solubility within the polymer are assumed to instantly equilibrate with
471 the external pressure, and these conditions are imposed via thermodynamic
472 equations (Eqn. 6). In our model, the increase in concentration at the

473 interface and in the polymer bulk are included in the form of physical
474 conversion processes.

475 Within each compartment in the bulk of the polymer, we use
476 computational constructs that are represented in Scheme 2. We use Ψ to
477 denote a polymeric matrix that can accommodate a certain concentration of
478 sorbed gas. The simplest implementation is in the single mode model
479 (Reaction 2A), in which the polymer that is initially under vacuum, Ψ_v , is
480 converted to a gas-exposed polymer, Ψ_p . The maximum concentration of
481 gas(p) sorbed within Ψ_p is determined by the final upstream pressure and the
482 gas solubility, and is calculated using Equation 1 or 2. The physical nature of
483 gas accommodation does not need to be defined within this model, only the
484 maximum sorbed gas concentration. Ψ_p (and therefore sorbed gas) is
485 uniformly distributed within each compartment. The rate coefficient for this
486 conversion process, k_{rise} , is set so that the time for Reaction 2A to be
487 completed is equal to the time for the pressure to rise, as done in a previous
488 study.¹² The values of k_{rise} are determined independently for each
489 experimental run due to variations in the pressure rise profile from run to
490 run; however, the same value of k_{rise} is used for each simulation of the same
491 experimental run (i.e., without swelling, with swelling, and concentration-
492 dependent diffusion). The rate law is zeroth order in polymer concentration,
493 and tracks only the pressure rise; any information on interactions between
494 the gas and polymer are contained within k_{rise} .

495

Change of Polymer from Vacuum to Pressurized Conditions

Single Mode Model



Dual Mode Model



497

498 **Scheme 2.** General scheme for the process by which the bulk polymer
 499 adjusts to the change in upstream pressure with their associated rate laws.
 500 The step for the single mode model (2A) is split into two separate steps (2B
 501 and 2C) for the dual mode model.

502

503 This description is generalized for the dual mode model by dividing Ψ_p
 504 between the dissolved mode, Ψ_p^D , and the Langmuir mode, Ψ_p^L , as shown in
 505 steps 2B and 2C, with the solubility within each mode calculated using the
 506 dual mode sorption parameters reported by Toi *et al.*⁴¹

507 5. Single-Mode Model

508 The single mode model treats all Ψ_p within the polymer as equivalent,
 509 similar to the treatment of permeation through rubbery polymers.¹² The
 510 diffusion coefficients for movement of solutes between compartments are
 511 calculated from the measured steady-state permeation data at each
 512 pressure using Equation 3.

513 **5A. Swelling**

514 Sorption of gases can lead to swelling, especially at high concentration.

515 We account for the dynamic change in volume of each compartment, i ,

516 during the simulation by calculating the current volume at each time step,

517 $V(t)$, using the equation

	$V(t) = \sum_i \frac{n_i(t)}{\rho_i}$	(9)
--	---------------------------------------	-----

518 where $n_i(t)$ is the amount of each substance at time t , and ρ_i is the molar

519 density of that substance. We assume that all species are incompressible

520 and that their occupied volumes are additive. The molar density ρ of the

521 polymer is calculated by dividing the mass density of the polymer by the

522 molar mass of its monomer, $m = 120$ g/mol in the case of PPO. This results in

523 $\rho = 8.83$ mol/L. The partial molar volume, V_p , of CO_2 in a glassy polymer

524 increases from 10 cm^3/mol in dilute form, and approaches 46 cm^3/mol (the

525 same as CO_2 in organic solvents) at high concentration.⁷¹ For this study, the

526 limiting cases of no swelling and maximum swelling ($V_p = 46$ cm^3/mol) are

527 tested.

528 More information on the effects of swelling is provided in SI Section 4.

529 **5B. Concentration-Dependent Diffusion**

530 Although the basic simulation assumes a constant diffusion coefficient,

531 it is possible that the diffusion coefficient early in the experiment, when the

532 polymer has been exposed to only a small concentration of gas, is different

533 from the apparent diffusion coefficient at steady state when the internal gas

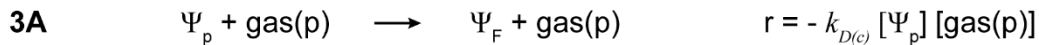
534 concentration is at its maximum. Such a scenario would imply a change in

535 polymer morphology, leading to Case II or anomalous diffusion at non-steady

536 state; at steady state, the experimental downstream pressure versus time
537 data have a constant slope, indicating that any changes within the polymer
538 have stabilized at that point. A computational scenario in which the diffusion
539 coefficient changes due to gas exposure has been tested in this work using
540 the method previously developed in Ref. ¹¹. The implementation is described
541 in Scheme 3, where the polymer converts from an initial form Ψ_p to a
542 subsequent form Ψ_F as the sorbed gas concentration increases using a
543 second order reaction step. The rate constant $k_{D(c)} = 6 \times 10^8 \text{ M}^{-1} \text{ s}^{-1}$ is
544 calculated by assuming a diffusion-controlled interaction between gas
545 molecule and a 1,3-dimethyl benzene monomer, as described in SI Section 3.
546 The presence of the 2 forms, Ψ_p and Ψ_F , creates two diffusion environments
547 that are treated as independent, parallel diffusion paths. Their relative
548 importance changes dynamically as the sorbed gas concentration increases.
549 Gas diffuses through the Ψ_p form with a diffusion coefficient that is equal to
550 the y-intercept in a linear fit to the experimental diffusion versus pressure
551 data (equation given in Figure 3), i.e. when the gas concentration is near
552 zero. The diffusion coefficient for gas through the Ψ_F form is the apparent
553 diffusion coefficient at steady state, $D_{app}(p_{up})$, given in Figure 3. It is possible
554 that the conversion from Ψ_p to Ψ_F is slow, i.e., reaction-controlled rather than
555 gas-diffusion controlled. This possibility was tested by reducing $k_{D(c)}$ over
556 several orders of magnitude (shown in SI Section 5), but those permeation
557 curves do not match the experimental data.

558

Concentration-Dependent Diffusion



559

560 **Scheme 3.** Reaction that alters the diffusion coefficient for the gases.

561

562 6. Dual-Mode Model

563 The dual mode model treats the sorbed gas within the polymer as two
564 different populations, dissolved and Langmuir. It is unknown whether the
565 same sorption mechanism governs dissolved and Langmuir populations, and
566 so three different scenarios are tested by adjusting k_{rise}^D and k_{rise}^L in Reactions
567 2B and 2C:

568 (i) Langmuir sorption is set to its maximum value from the start of the
569 simulation, dissolved sorption increases with the pressure rise (Ψ_p^L is present
570 from the start, and Reaction 2C is omitted).

571 (ii) Both dissolved and Langmuir sorption increase simultaneously ($k_{rise}^D =$
572 k_{rise}^L).

573 (iii) Dissolved and Langmuir sorption increase on different timescales (k_{rise}^D
574 $\neq k_{rise}^L$).

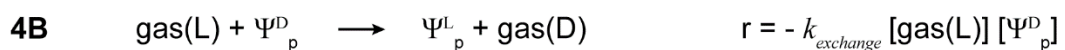
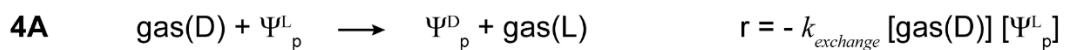
575 Scenario (i) is most consistent with a strict interpretation of the dual mode
576 model, where the void spaces for Langmuir sorption are an inherent part of
577 the material structure, similar to zeolites. The other two scenarios include
578 the possibility that the interactions between polymer and gas affect the

579 polymer structure and dynamics. In Scenario (ii), the two sorption modes
 580 respond similarly to gas absorption, whereas in Scenario (iii), they respond
 581 differently. The values of k_{rise}^D and k_{rise}^L are determined as fitting parameters
 582 that produce the correct downstream pressure versus time curves.

583 Typically, it is assumed that there is continuous, diffusion-controlled
 584 interchange of solutes between the two sorption modes. The rate coefficient
 585 for exchange between site types, $k_{exchange}$, was calculated from the
 586 Smoluchowski equation for a diffusion-controlled reaction, as detailed in the
 587 SI Section 3, resulting in $k_{exchange} = 2 \times 10^7 \text{ M}^{-1} \text{ s}^{-1}$. However, using this value
 588 produces an inefficient simulation where most of the computation time was
 589 being spent shuffling molecules between dissolved and Langmuir sites, a
 590 drawback of the simulation method. Therefore, for computational efficiency,
 591 we allow $k_{exchange}$ to be a much smaller value, $10^2 \text{ M}^{-1} \text{ s}^{-1}$. The impact of this
 592 assumption was tested by running some of the simulations with $k_{exchange} = 10^3$
 593 $\text{M}^{-1} \text{ s}^{-1}$ and $k_{exchange} = 10^4 \text{ M}^{-1} \text{ s}^{-1}$, and the results were identical (shown in SI
 594 Section 6). The insensitivity of the simulations to $k_{exchange}$ indicates that the
 595 exchange process is not kinetically controlling.

596

Exchange Between Sorbed Gas Populations



597

598 **Scheme 4.** Reactions for the exchange of gases between the dissolved (ψ_p^D)
599 and Langmuir (ψ_p^L) sorption modes.

600

601

602 Results

603 1. Experiment

604 1A. PPO Membrane Properties

605 The density of the PPO membranes is measured to be 1.06 ± 0.09
606 g/cm^3 , which gives a FFV of 0.190.⁴²⁻⁴³ The Tg is $214 \pm 7^\circ\text{C}$. Compared to
607 literature data, our samples have a lower density and a Tg in the middle of
608 the range reported.^{20, 41, 43, 46, 72-80} The large deviation in Tg is due to the broad
609 peak in the DSC scans. The crystallinity is calculated to be 20.6%; reports of
610 PPO crystallinity in the literature are rare, and the few reported values vary
611 widely from 3% to 48%.^{73, 79}

612

613 1B. Permeation Measurements

614 Sorption and permeability data are presented in Figure 3. The
615 permeability coefficients, P_m , are calculated for each run from Equation 4 for
616 upstream pressures, p_{up} , ranging from 1-18 atm, and are plotted in Figure 3b.
617 The raw data for downstream pressure versus time from which P_m are
618 calculated are presented in the SI Section 7, Figures S8 - S9. Changes in
619 downstream pressure due to gas leaks, $(dp_{ds}/dt)_{leak}$, are less than 5% in all
620 cases. The permeability coefficients for N_2 are consistent with previous
621 reports from Toi *et al.*⁴¹ The permeability coefficients for CO_2 in this study are

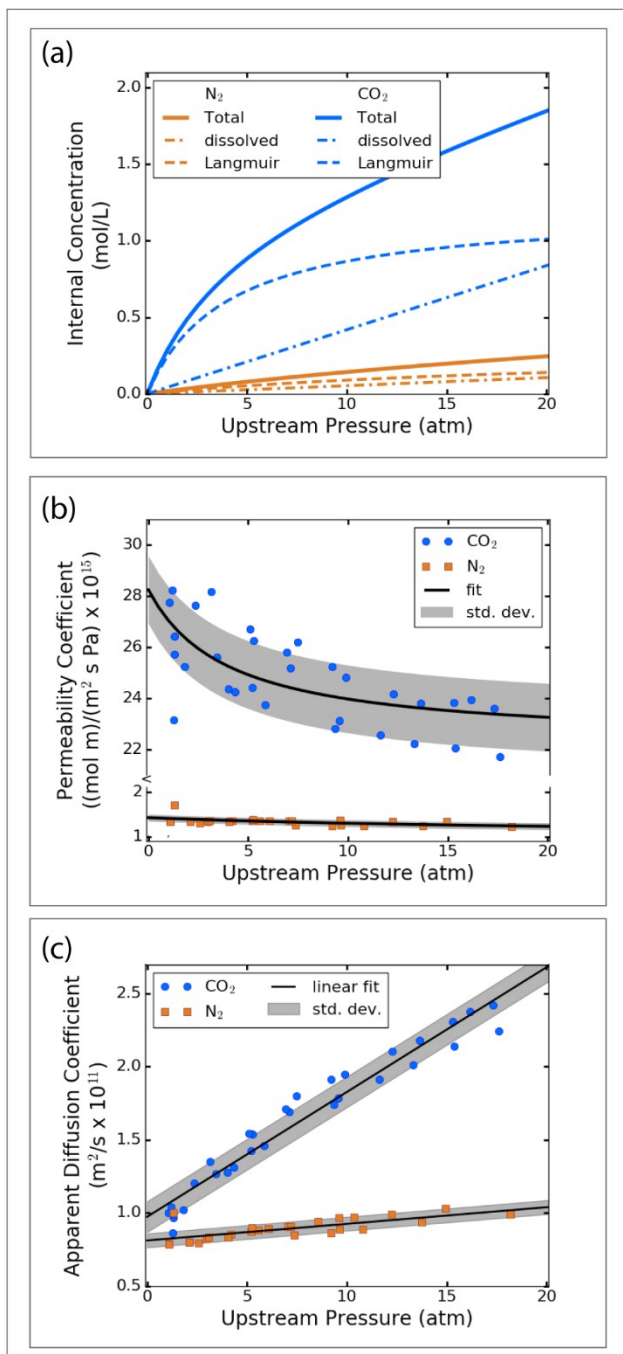
622 slightly greater than other values reported in the literature (see SI Section
623 1).^{20, 24, 41, 46, 72, 79} Our analysis of data from Wright and Paul⁴⁶ shows that
624 permeability decreases with increasing density, but has a non-monotonic
625 relation to T_g (details in SI Section 8). Because our samples have a low
626 density, though still within the range reported in other studies, it is to be
627 expected that they will have a higher permeability. Both solubility and
628 diffusivity of CO_2 in PPO are higher than N_2 , even though CO_2 is the larger
629 molecule.

630

631 1C. Diffusion Coefficient Determinations

632 The measured steady state permeation data are fit with both the dual
633 and single mode models to extract diffusion coefficients for the simulations.
634 Results using the dual mode model for permeation (Eqn. 3 and Figures 3a
635 and 3b) are listed in Table 4 and are used in the dual mode multiscale
636 simulations. The standard deviation represents $\pm 5.5\%$ and $\pm 4.7\%$ from the
637 non-linear dual mode fit for N_2 and CO_2 , respectively. The assumption that
638 there is a simple linear relation between P and p_{up} (shown in SI Section 9
639 Figure S11) results in no change to the standard deviation, indicating that
640 the more complex non-linear fitting of the dual mode model may not be
641 necessary. Recalculating the permeability coefficients using the final
642 thickness predicted by simulations (i.e., accounting for swelling) changes
643 their values by $<5\%$.

644



645

646 **Figure 3.** Isotherms as a function of upstream pressure. (a) Dual mode
 647 sorption, using the sorption isotherms from Ref. ⁴¹ The total sorbed gas
 648 concentration (solid lines) is divided into the dissolved mode (dot-dash lines)
 649 and the Langmuir mode (dashed lines). (b) Dual mode permeability values
 650 for N_2 (orange squares) and CO_2 (blue circles), shown for all PPO samples.

651 The black lines are a fit using with parameters listed in Tables 3 and 4. The
652 gray area shows one standard deviation. (c) Single mode apparent diffusion
653 coefficients calculated using data in (b).

654

655 Single mode apparent diffusion coefficients, D_{app} , were calculated using
656 data in Figure 3b, Eqn 1, and S_d from Table 3. For both N_2 and CO_2 , D_{app}
657 increases with increasing pressure, indicating that the presence of gas
658 changes the environment within the polymer to ease transport of additional
659 gas. D_{app} vary linearly with p_{up} , with $D(CO_2)=(0.0853 p_{up}+0.974) \times 10^{-11}$ m²/s,
660 11 % standard deviation, and $D(N_2)=(0.0114 p_{up}+0.812) \times 10^{-11}$ m²/s, 5.9 %
661 standard deviation.

662

663 **Table 4.** Diffusion coefficients for N_2 and CO_2 in PPO, by fitting the
664 experimental permeability data with the dual mode permeation model (Eqn
665 6).

	D_d	D_L
	m ² /s	m ² /s
N_2	1.886×10^{-11}	3.528×10^{-12}
CO_2	5.391×10^{-11}	2.003×10^{-12}

666

667 2. Molecular Dynamics

668 The density of the polymer in the MD simulations is 1.01 g/cm³, which
669 is lower than the 1.06 g/cm³ in the experiment. This discrepancy is most

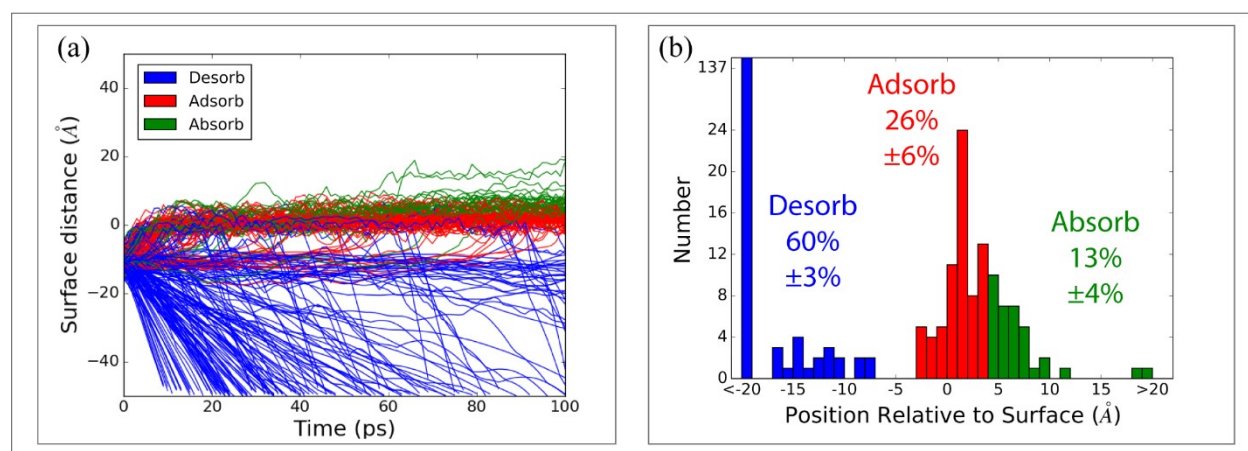
670 likely due to the short chain lengths (100 monomers) and the small thickness
671 (< 6 nm) used for the MD study. Currently, it is necessary to simulate small
672 systems due to the computationally intensive nature of MD. Because of these
673 limitations, we use the results of the MD studies in a limited manner.

674 2A. Interfacial Sticking Probabilities

675 The sticking coefficient refers to a kinetic factor, the probability of a
676 gas impinging on a surface to remain on the surface. It is distinct from the
677 solubility or uptake, which is the probability for a molecule in the gas phase
678 to move into the bulk region of the polymer.⁸¹ Results of the molecular
679 dynamics simulations to determine a sticking coefficient for CO₂ on PPO are
680 shown in Figure 4. Trajectories are classified as representing adsorption,
681 desorption and absorption events based on the position of the CO₂ molecule
682 at the end of 100 ps. Some care must be taken in how the classification of
683 type of event is interpreted: the distinction between an adsorbed and
684 absorbed molecule is arbitrary, especially for atoms just below the gas-
685 polymer interface, and the fate of molecules adsorbed on the surface is not
686 clear from the finite simulation time. Thus, sticking in these simulations has
687 a lower bound of 13%, equal to the fraction of absorbed molecules, and an
688 upper bound of 40%, equal to the fraction of absorbed plus adsorbed
689 molecules.

690 The minimum sticking coefficient of $\mu = 13\%$ is used in the reaction-
691 diffusion simulations for all gas molecules. This value is lower than our
692 previous findings for CO₂ sticking to the surface of poly(dimethyl siloxane)
693 (PDMS) of 30%¹² but is within the range of 10% to 100% found in other

694 systems studied by molecular dynamics (MD) at room temperature.^{51-52, 82-84}
695 Our previous study showed that the multiscale model is insensitive to the
696 precise value of the sticking coefficient over a range of several orders of
697 magnitude, and so any errors due to the low density or slight differences
698 between CO₂ and N₂ will not affect the multiscale modeling results. The
699 interaction that determines how well a gas molecule will stick to a polymer
700 surface is not well understood, and the data collected in this study did not
701 provide any additional insights beyond what has already been published.^{51-52,}
702 ⁸³⁻⁸⁵
703



704
705 **Figure 4.** Results of the molecular dynamics simulations of CO₂ sticking to
706 PPO. For both panels the surface is defined as position 0 with positive
707 positions occupied by the polymer and negative positions corresponding to
708 an empty region. (a) Distance from the instantaneous surface as a function
709 of time for all 265 trajectories. (b) Histogram of outcomes from all CO₂
710 impacts onto the PPO surface.

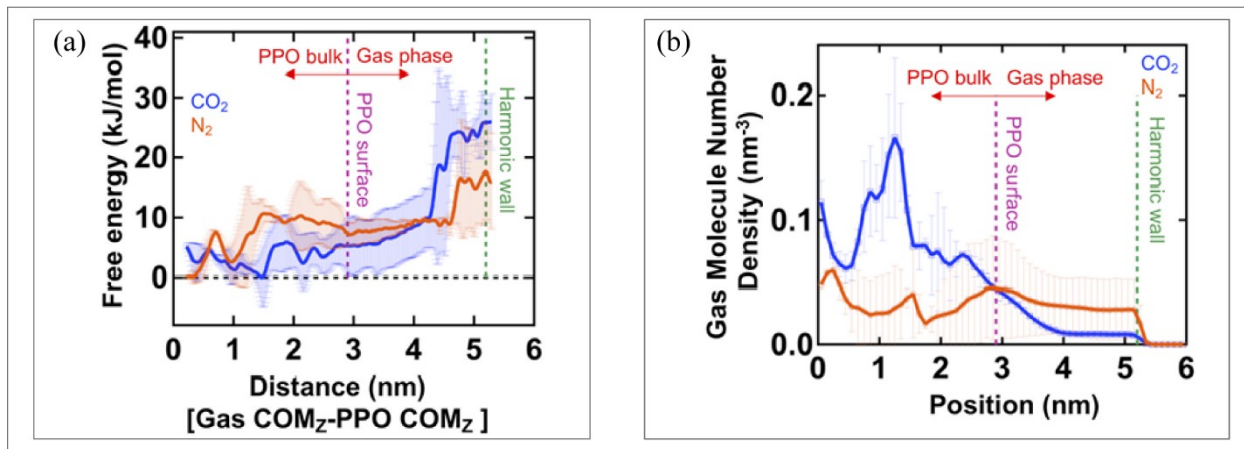
711

712 2B. Free Energy Profile

713 The results of the free energy calculations are reported in Figure 5. In
714 Figure 5a, both CO₂ and N₂ have a higher (less favorable) free energy in the
715 gas phase. The variations in the gas phase free energy are due to
716 interactions with other gas molecules and to long-ranged electrostatic and
717 van der Waals interactions with the polymer. Both gases experience a
718 decrease in free energy in the surface region of the polymer compared to the
719 gas phase. The decrease in free energy is due to enthalpy, since entropy
720 should decrease upon gas sorption into the polymer; additional studies at
721 other temperatures would be required to determine the precise entropic
722 contributions to the free energy change. N₂ appears to have a greater affinity
723 for the surface region, whereas CO₂ finds the surface less favorable than the
724 bulk, though for both gases, their most favorable position (minimum free
725 energy of 0 kJ/mol) is located in the bulk. The difference in free energy
726 between the gas phase and the bulk region gives the affinity of the gas for
727 the polymer; CO₂ has a stronger affinity of ~18 kJ/mol compared to 7 kJ/mol
728 for N₂. Qualitatively similar results are seen in the number density of gas
729 molecules based on position shown in Figure 5b. The density profiles
730 demonstrate that both CO₂ and N₂ have the same density at the surface.
731 However, the greatest number of N₂ molecules, on average 2.2 out of 4 N₂
732 molecules, reside in the gas phase, implying that they favor a position near
733 the PPO surface but not in contact with it. In contrast, a greater number of
734 CO₂ molecules, on average 3.2 out of 4 CO₂ molecules, exist in the PPO bulk.

735 The free energy profile (Fig. 5a) for CO₂ in the PPO bulk features several ups
736 (peaks) and downs (basins) with moderate energy barriers separating the
737 states. Moderate energy barriers allow CO₂ to hop more frequently between
738 the open spaces during polymer segmental motion. In contrast, N₂ has fewer
739 peaks/basins but with high energy barriers, especially near the center of
740 mass of the polymer, suggesting that the trapped N₂ molecules wait longer
741 for a forward jump. The diffusion of N₂ and CO₂ is depicted in SI Section 10 in
742 Figures S12 and S13, which confirm that CO₂ has larger displacements more
743 frequently than N₂ and supports the idea that the higher diffusivity of CO₂
744 over N₂ can be attributed to its more frequent jumps within the polymer
745 structure. Figures S12c-f and S13c-f show that CO₂ passes through the entire
746 PPO slab 20 times in total but N₂ has only 1 successful pass, which suggests
747 that CO₂ has 20 times greater permeability over N₂. This value is remarkably
748 (and perhaps fortuitously) close to ratio of the experimental permeabilities of
749 19 at 2 atm. While the absolute values of free energy may shift if the
750 polymer density were closer to the experimental value, the comparative
751 behavior of N₂ and CO₂ should remain valid.

752



753

754 **Figure 5.** (a) Free energy profile of the biased N₂ (orange) and CO₂ (blue)
 755 molecule as a function of distance in the z-direction between the center of
 756 mass (COM) of the gas molecule and the COM of PPO. (b) Number density of
 757 the non-biased N₂ (orange) and CO₂ (blue) molecules with respect to position
 758 in the z-direction, which is normal to the surface of the polymer slab where 0
 759 is the center of polymer. Both plots show the average and standard deviation
 760 between positive and negative z-positions. The surface position is defined as
 761 the point at which the PPO density falls to half of its bulk value, averaged
 762 between the CO₂ and N₂ systems. The surface width, as defined by the
 763 distance between the 10% and 90% density positions in the “10-90” Gibbs
 764 division surface definition is 1.3 and 1.4 nm for the CO₂-PPO and the N₂-PPO
 765 system, respectively.

766

767 3. Multi-Scale Reaction-Diffusion Simulations, Single Mode Model

768 The result of the simulations of PPO permeation by N₂ and CO₂ are
 769 presented as the downstream pressure versus time and compared to
 770 experiment in Figures 6-9 for the single mode model and its variations. The

771 results for a membrane thickness of 22.4 μm with $p_{up}(\text{CO}_2) = 1.82 \text{ atm}$ and
772 $p_{up}(\text{N}_2) = 7.38 \text{ atm}$ are presented in the main text because they display the
773 largest difference between rubbery and glassy behaviors. The input values
774 used are listed in Table 5. Additional figures showing similar findings for
775 other membrane thicknesses and gas pressures are provided in SI Section
776 11.

777 For N_2 (Fig. 6a, 7a, 8a, 9a), the upstream pressure rises in 3.13 s. If the
778 polymer conversion process (Model Development section 4) is also
779 completed in 3.13 s, indicating an instantaneous equilibration between
780 upstream pressure and internal polymer state, then the simulated pre-steady
781 state downstream pressure does not agree with experiment. Figure 6a
782 compares such an instantaneous response to the response calculated when
783 k_{rise} is treated as an adjustable (non-instantaneous) parameter that brings
784 the simulation results for pre-steady state into agreement with the
785 experiment. As seen in Table 5, the non-instantaneous value for k_{rise} is
786 smaller than the instantaneous value, and the conversion reaction is slower.
787 We estimate that completion of the polymer conversion reaction (Reaction
788 2A) for maximum gas uptake requires 24.0 s for N_2 under these specific
789 experimental conditions. Similarly, for CO_2 (Fig. 6b, 7b, 8b, 9b), the upstream
790 pressure rises over the course of 2.08 s, but the polymer conversion is
791 completed at 17.4 s in the simulations that match experiment. This indicates
792 that for both gases the equilibration of the polymer with the upstream gas
793 pressure is delayed, in contrast to the standard assumption of instantaneous

794 equilibration and in contrast to the previously observed behavior in rubbery
 795 polymers.¹² The experimental apparatus is the same as that used in the
 796 rubbery polymer work,¹² so if the delay were due to instrumental artifacts, it
 797 would have been seen in the earlier work as well.

798 The values of k_{rise} for instantaneous and non-instantaneous
 799 equilibration for both gases were determined using the swelling single mode
 800 model, and then the same set was used for the constant volume and
 801 concentration-dependent diffusion coefficient simulations.

802

803 **Table 5.** Inputs for single mode simulations

		N ₂	CO ₂
Sample		2	2
p_{up}	atm	7.38	1.82
$[gas(g)]_{init}$	mol/L	5.20×10^{-7}	4.68×10^{-7}
$[gas(p)]_{max}$ in Ψ_p	mol/L	0.110	0.4554
k_{rise} (instantaneous)	M s ⁻¹	0.1	0.5
k_{rise} (non- instantaneous)	M s ⁻¹	0.007	0.035
D_{app}	m ² /s	8.494×10^{-12}	1.023×10^{-11}

804

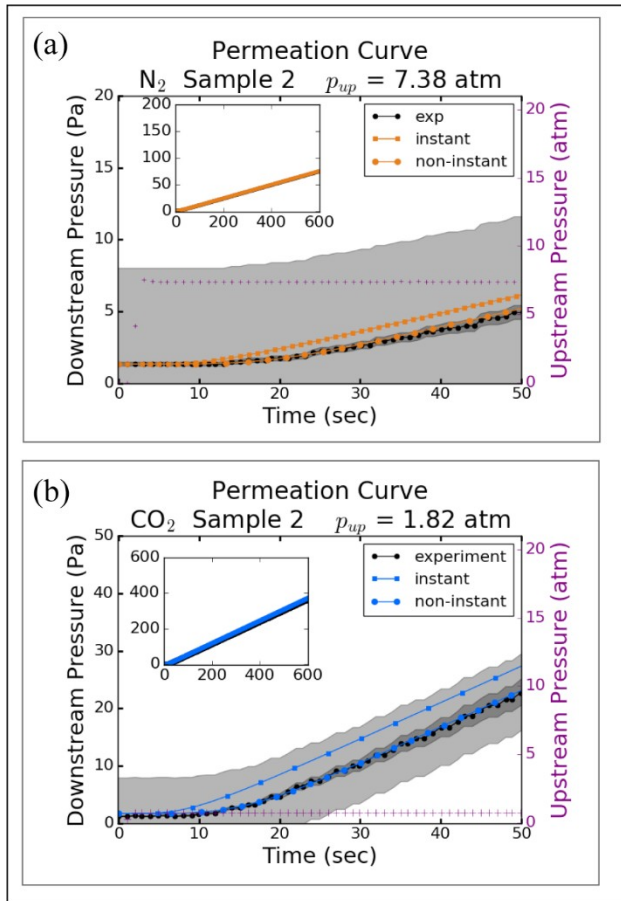
805

806 3A. Single Mode Model with Constant Volume

807 Permeation curves for the single mode model without swelling are
 808 shown in Figure 6. The assumption of instantaneous equilibration leads to

809 erroneous pre-steady state behavior, whereas non-instantaneous
810 equilibration matches experiment at both pre-steady and steady state.

811



812

813 **Figure 6.** Permeation curves for the single mode model without swelling for

814 (a) N₂ and (b) CO₂ using instantaneous (squares) and non-instantaneous

815 (circles) equilibration between the external pressure and bulk polymer state.

816 The gray region represents a measurement error of approximately 10%.

817 Note that the axes' scales are different for N₂ and CO₂ so that the details in

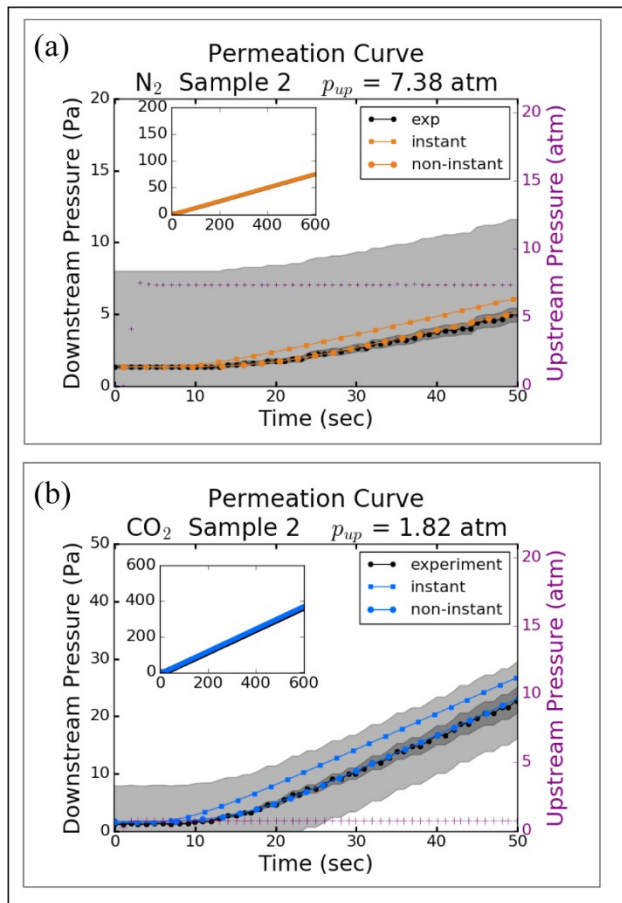
818 both sets of curves can be seen.

819

820 3B. Single Mode Model with Swelling

821 Permeation curves for the single mode model with the maximum
822 amount of swelling are shown in Figure 7. Again, the assumption that
823 equilibration between the bulk polymer and upstream pressure is
824 instantaneous leads to incorrect pre-steady state behavior. Assuming a non-
825 instantaneous response results in simulations that match experiment. The
826 effect of swelling on the permeation kinetics is negligible.

827



828

829 **Figure 7.** Permeation curves for the single mode model with the maximum
830 amount of swelling for (a) N₂ and (b) CO₂ using instantaneous (squares) and
831 non-instantaneous (circles) equilibration between the external pressure and

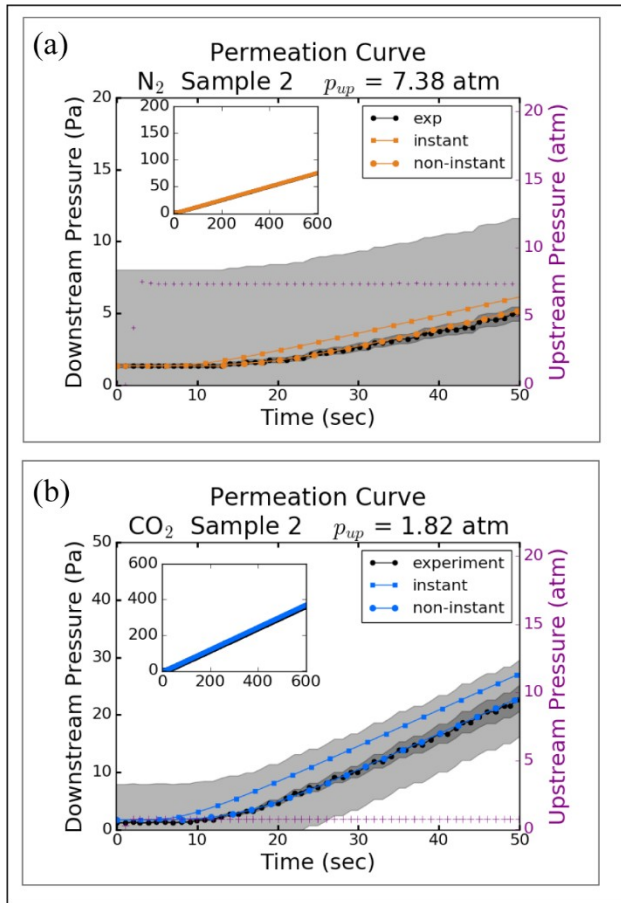
832 bulk polymer state. The gray region represents a measurement error of
833 approximately 10%. Note that the axes' scales are different for N₂ and CO₂ so
834 that the details in both sets of curves can be seen.

835

836 3C. Single Mode Model with Concentration-Dependent Diffusion

837 We tested the possibility that the steady-state pressure-dependent
838 diffusion coefficients shown in Figure 3c are incorrect during the pre-steady-
839 state regime, i.e. are dependent on local gas concentration in the polymer
840 during the pressure rise. This is an alternative explanation for the
841 discrepancy between instantaneous response predictions and experimental
842 observations. Simulation results using the method and diffusion coefficients
843 described in Model Development Section 5b and SI Section 5 for the single
844 mode model with swelling are shown in Figure 8. It is evident that even with
845 concentration-dependent diffusion coefficients, assumption of a non-
846 instantaneous equilibration of the bulk polymer to the upstream pressure
847 increase is necessary to match experiment. These results show that swelling
848 and concentration-dependent diffusion do not account for pre-steady-state
849 permeation behavior.

850



851

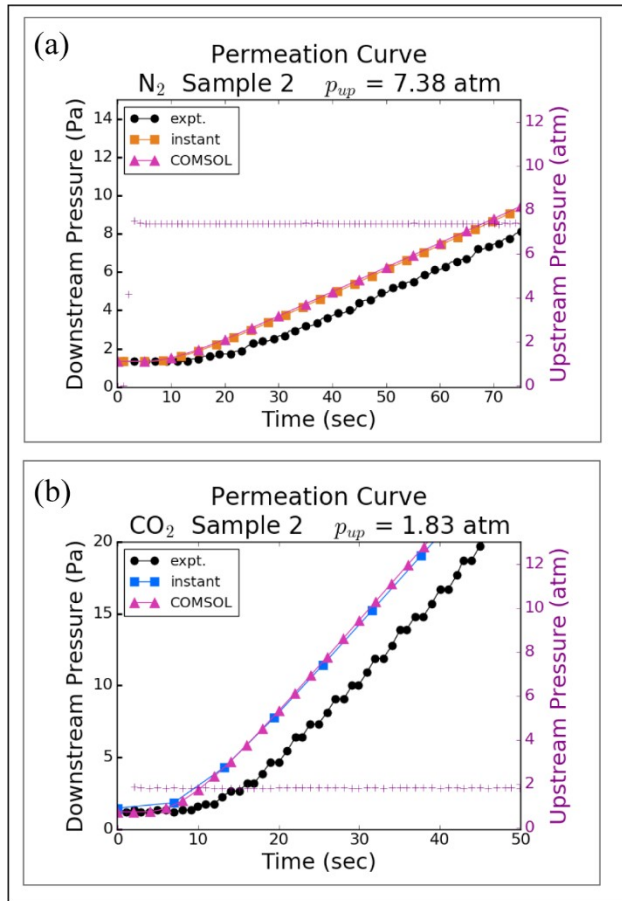
852 **Figure 8.** Permeation curves for the single mode model with swelling and
 853 gas concentration-dependent diffusion for (a) N₂ and (b) CO₂ using
 854 instantaneous (squares) and non-instantaneous (circles) equilibration
 855 between the external pressure and bulk polymer state. The gray region
 856 represents a measurement error of approximately 10%. Note that the axes'
 857 scales are different for N₂ and CO₂ so that the details in both sets of curves
 858 can be seen.

859

860 3D. Delayed Polymer Response in the Single Mode Model

861 Non-instantaneous equilibration between the bulk polymer and the
 862 external pressure during pre-steady state gas permeation has not been

863 previously reported. In order to rule out any potential artifacts from our
864 simulation methodology, deterministic multi-physics simulations using
865 COMSOL⁸⁶ were performed to predict the permeation curves (Fig. 9). Both
866 deterministic and stochastic simulations predict incorrect pre-steady state
867 behavior if instantaneous equilibration is assumed.

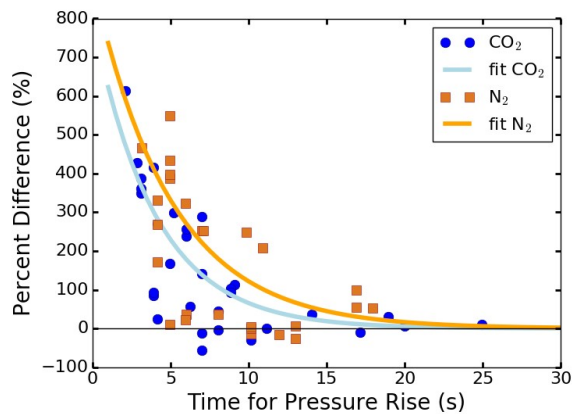


868
869 **Figure 9.** Comparison of permeation curves for (a) N₂ and (b) CO₂ from
870 different modeling approaches. The results from COMSOL match the
871 (Kineticscope) model with instantaneous equilibration and no swelling. Note
872 that the axes' scales are different for N₂ and CO₂ so that the details in both
873 sets of curves can be seen.

874 Figures S14 - S16 in SI Section 11 present simulation results in
875 comparison to experiment for a full range of upstream gas pressures. k_{rise}
876 was determined independently for each experimental run, values are
877 presented in Table S2.

878 Using these results, we calculated the percent difference in the
879 timescales to reach the maximum solute concentration within the polymer
880 and to reach the maximum upstream pressure. A percent difference of zero
881 at all times would correspond to instantaneous equilibration. What is found is
882 that the percent difference is very large when the pressure rise time is short,
883 and decreases exponentially with increasing pressure rise time for both
884 gases, as shown in Figure 10. The behavior in Figure 10 is consistent with
885 ideas from linear response theory (LRT),⁸⁷ if we consider the polymer to be in
886 a pseudo-equilibrium state before the gas is introduced in the experiment,
887 and after the gas pressure reaches steady state. LRT says that when the
888 state of a system strongly driven, such as with a rapid change in pressure,
889 the system will take some time to relax to its new equilibrium state. In
890 contrast, a weakly driven system, such as with a slow pressure rise, can be
891 considered as a pseudo-equilibrium system throughout the course of the
892 state change. The results in Figure 10, when combined with the data in
893 Figure 3c showing that the pressure-dependence of the diffusion coefficients
894 for N_2 is much weaker than for CO_2 , point to the relaxation time as being
895 characteristic of the PPO-gas combination. It should be noted that this
896 relaxation occurs even when the solute is inert to the polymer (N_2),

897 suggesting that the mere presence of the solute affects polymer structure.
898 Although it appears from Figure 10 that the polymer response could possibly
899 be somewhat slower in the presence of N₂, the scatter in the data is too large
900 to make this claim.
901



902
903 **Figure 10.** Percent difference between the time for the increase in pressure-
904 dependent maximum concentration in the polymer and the upstream
905 pressure rise time for CO₂ (blue circles) and N₂ (orange squares) as a
906 function of upstream pressure rise time. The solid lines are an exponential
907 decay fit to the data where $y(CO_2)=800e^{-0.25x}$ and $y(N_2)=900e^{-0.20x}$.

908
909 Throughout this work, the rate coefficient, k_{rise} , is used as an adjustable
910 parameter and does not correspond to a primary process. We can
911 hypothesize that k_{rise} contains contributions from the rate of pressure
912 increase, the final pressure, polymer response, etc. To investigate the
913 physical mechanism and determine a series of elementary steps for the

914 polymer conversion process, we would need to develop new instrumentation
915 to record detailed information on the dose-response timings in this system
916 and on sample-to-sample variations, accompanied by in situ modulus
917 measurements. We suggest that new experimental work of this type would
918 be invaluable for gaining new insights to gas-polymer interactions. The
919 multiscale model framework described here can be readily extended to
920 include additional details, and would help develop a robust connection
921 between permeation theory and data. This would allow apparent, pressure-
922 dependent diffusion coefficients to be directly and quantitatively linked to
923 polymer relaxation processes.

924

925 4. Multi-Scale Reaction-Diffusion Simulations, Dual Mode Model

926 In the dual mode model, the sorbed gas is split into 2 populations,
927 gas(D) and gas(L), which are associated with ψ_p^D and ψ_p^L , respectively. As in
928 the single mode model, neither the precise nature of the polymer matrix nor
929 the physical nature of gas accommodation need to be specified. The gas
930 associated with each mode is treated as being distributed evenly throughout
931 the compartment.

932 Three possible scenarios for how the polymer matrix adjusts to the
933 pressure rise are tested, as described in Model Development Section 6. The
934 input variables for the dual mode simulations of N₂ at 18.18 atm and CO₂ at
935 17.23 atm are listed in Table 6, and the associated values for k_{rise}^D and k_{rise}^L
936 are listed in Table 7. As shown in Figure 11, each of the scenarios can

937 properly describe the pre-steady state downstream pressure increase. The
 938 results of additional dual mode simulations are shown in SI Section 12,
 939 together with the corresponding input variables.

940 The contribution of the dissolved and Langmuir modes to transport
 941 depends on the concentration gradient of sorbed gas within their respective
 942 populations multiplied by their characteristic diffusion coefficient. In all
 943 cases, the dissolved mode diffusion coefficient, D_d , is much larger than the
 944 Langmuir diffusion coefficient, D_L (see Table 4). Therefore, when the solute
 945 concentration profile of each type in the polymer is similar, most of the flux
 946 occurs via the dissolved mode due to its higher diffusion coefficient. On the
 947 other hand, when the Langmuir-type concentration is much larger than the
 948 dissolved concentration, like at low pressures (see Fig. 3a), most of the
 949 permeation flux is by the Langmuir mode due to its higher concentration
 950 gradient.

951

952 **Table 6.** Values of input variables for the dual mode simulations.

		N ₂	CO ₂
Sample		4	3
p_{up}	atm	18.18	17.23
$[\text{gas(g)}]_{\text{init}}$	mol/L	3.64 × 10 ⁻⁷	4.16 × 10 ⁻⁷
$[\text{gas(p)}]_{\text{max}}$ in ψ_p^D	mol/L	0.0960	0.725
$[\text{gas(p)}]_{\text{max}}$ in ψ_p^L	mol/L	0.132	0.984

953

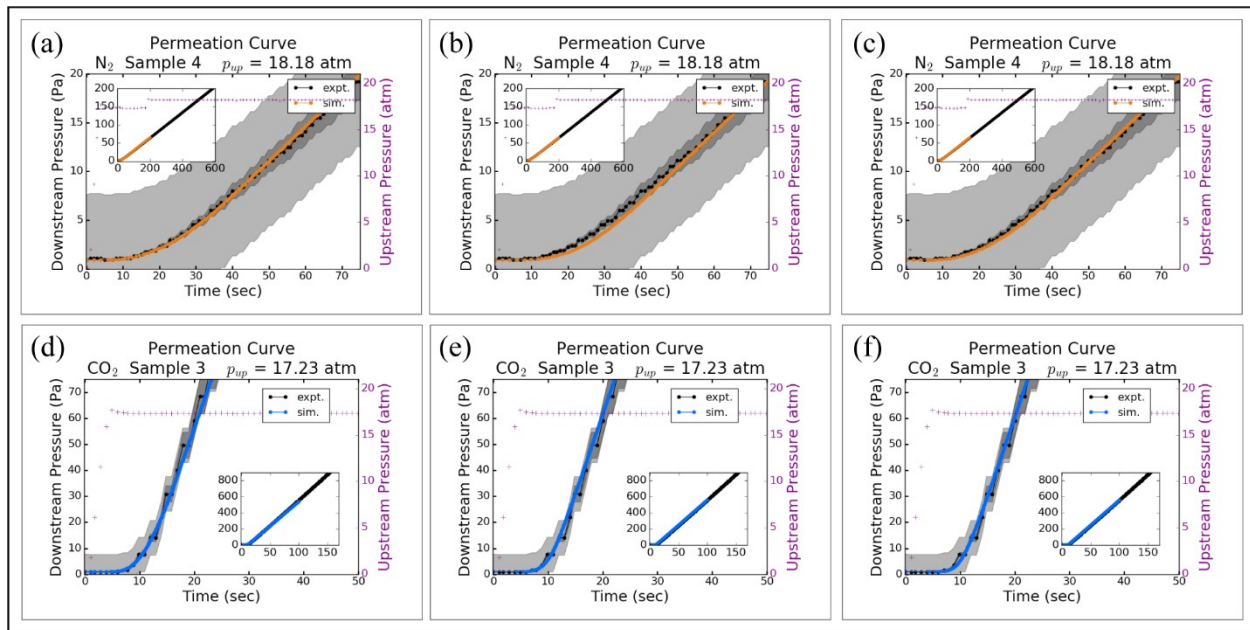
954

955 **Table 7.** Values of k_{rise}^D and k_{rise}^L for Scenarios (i) - (iii) of the dual mode
 956 model for the sample number and upstream pressure shown in Figure 11.

Scenario	N ₂		CO ₂	
	k_{rise}^D	k_{rise}^L	k_{rise}^D	k_{rise}^L
	M s ⁻¹	M s ⁻¹	M s ⁻¹	M s ⁻¹
(i)	0.003	n/a	0.06	n/a
(ii)	0.004	0.004	0.08	0.08
(iii)	0.003	0.1	0.06	0.1

957

958



959

960 **Figure 11.** Permeation curves for (a-c) N₂ (orange) and (d-f) CO₂ (blue) with
 961 three different descriptions of the increase in maximum permeant
 962 concentration in the polymer: (a,d) Scenario (i) in which Langmuir sorption
 963 can occur from the start of the simulation, but dissolved sorption is related to

964 the pressure rise. (b,e) Scenario (ii) in which both dissolved and Langmuir
965 sorption increase at the same time. (c,f) Scenario (iii) in which dissolved and
966 Langmuir sorption increase on different timescales. The gray region
967 represents a measurement error of approximately 10%. Note that the axes'
968 scales are different for N₂ and CO₂ so that the details in both sets of curves
969 can be seen.

970

971 Discussion

972 This work seeks to develop and validate a single computational
973 framework for simulation of permeation of gases through glassy polymers
974 under both non-steady-state and steady-state conditions. We have examined
975 two main permeation models for this framework - single and dual mode -
976 with several variations of each. By comparing simulations to experiments, we
977 find that the full time-dependent permeation behavior can only be accounted
978 for by incorporating non-instantaneous equilibration between external
979 pressure and the maximum solute uptake of the polymer into the framework.
980 Neither swelling nor concentration-dependent diffusion coefficients can
981 account for the observations. In addition, the simulation results indicate that
982 both the dual mode and single mode models can correctly reproduce
983 experimental data. Accordingly, the dual mode model has no advantages
984 over a single mode model for accurately capturing time-dependent
985 permeation, but has disadvantages in terms of added model complexity.
986 Minelli and Sarti have similarly shown the adequacy of a single transport

987 mode using the non-equilibrium lattice fluid model (NELF) model.⁸⁸⁻⁸⁹ The
988 present work adds to a growing body of work that calls into question a
989 physical interpretation of the dual mode model.

990 In general, the values for solubility and diffusivity (S_d , S_L , b_L , D_d , D_L) in
991 the dual mode model are found by a non-linear fit to Equations 2 and 3. The
992 values of these parameters are non-unique, i.e., multiple sets of values can
993 fit the experimental isotherms equally well (SI Section 1).^{20, 24, 41} Moreover,
994 the best-fit values also depend on the pressure range over which the
995 isotherms are investigated, with an increase in S_L and decreases in S_d and b_L
996 as the upper end of the range increases.²⁵ While these parameters can be
997 correlated with a variety of physical properties of the polymer and gas (e.g.,
998 T_g , FFV, $\rho(\text{gas}_{(p)})$), the correlations are weak due to a large degree of scatter
999 in the data, especially when comparing between different structural families
1000 (e.g., poly(phenylene oxides) vs polysulfones).²⁶ Typically, the dissolved
1001 mode diffusion coefficient is an order of magnitude faster than the Langmuir
1002 diffusion coefficient.^{41, 90-93} While coefficient values could correspond to two
1003 different fluctuation modes of the polymer, there is no *a priori* reason to
1004 associate one parameter with the dissolved mode and the other with the
1005 Langmuir mode. Furthermore, the dual mode model treats transfer between
1006 dissolved and Langmuir sites as instantaneous, so it is unclear how each of
1007 these two modes could contribute uniquely to transport. Moreover, the
1008 diffusion coefficients are uncorrelated with the critical volume of the gaseous
1009 permeants. Therefore, it appears that the dual mode solubility and diffusivity

1010 values should be treated simply as empirical fitting parameters and not
1011 literally indicating two additive modes of sorption and transport at the
1012 molecular level.

1013 Experimentally, it is observed that the volume of polymers decreases
1014 more slowly with decreasing temperature below the glass transition
1015 temperature than above it.¹⁴⁻¹⁵ The difference between the glassy volume
1016 and a hypothetical rubbery volume at that temperature is defined as the
1017 excess free volume. Using positron annihilation lifetime spectroscopy (PALS),
1018 the excess free volume is shown to appear as an increase in magnitude of
1019 both the FFV and the FVE size in pristine glassy polymers.¹⁸ Although the
1020 dual mode model is not clearly connected to physical properties of the gas-
1021 polymer systems, it does raise the question of whether excess free volume in
1022 glasses contributes to permeation in a manner that is different from that for
1023 free volume in rubbers.

1024 If glassy polymer permeation consists of filling pre-formed voids,
1025 analogous to the internal space in zeolites, then simple space-filling
1026 arguments should account for the majority of sorption. However, the amount
1027 of N₂ sorbed via the Langmuir mode in a dual-mode analysis is typically less
1028 than the amount of CO₂,^{41, 90, 93} even though N₂ has the smaller critical
1029 volume. We use molecular dimensions in our analysis because they describe
1030 a fundamental molecular property, the space occupied by a molecule's
1031 electron cloud. Though the kinetic diameters are commonly used in the

1032 polymer membrane community, those values are based on equilibrium
1033 sorption into zeolites,⁹⁴ a scenario that is not necessarily directly translatable
1034 to diffusion through polymers. Furthermore, the kinetic diameter is often
1035 thought of as a shape correction for oblong molecules, but this correction is
1036 not applied consistently. For example, both N₂O and CO have the same
1037 length-to-width ratio (see Table S6), but only one of them receives a shape
1038 correction in the original work of Breck.⁹⁴ While the kinetic diameter is
1039 convenient for placing CO₂ within the trends for *P* and *D* versus size of other
1040 light gases, based on the considerations described here, it should not be viewed
1041 as a fundamental molecular property (see SI Section 13 for further discussion
1042 of this point).

1043 Furthermore, PALS studies on polycarbonate²⁷ and polysulfone²⁸ show
1044 that the FFV and FVE size distribution are not inert properties of the polymer
1045 material but can increase with sorption of CO₂. So even though CO₂ is filling
1046 some void space, it is also inducing a polymer relaxation that creates
1047 additional void space. The additional void space may be created by an
1048 increase in spacing between polymer segments that has been observed with
1049 wide angle x-ray diffraction (WAXD) after CO₂ sorption into poly(methyl
1050 methacrylate) and polycarbonate.³³ In the same study,³³ N₂ was shown to
1051 decrease the spacing between polymer segments, which may be the reason
1052 for its lower diffusion coefficient. The amount of void space created in
1053 polysulfone by CO₂ decreases slowly (over 10 hours) during exposure to
1054 vacuum.²⁸ Though the diffusion coefficient is known to increase with an

1055 increasing amount of FFV at steady state,²⁰ the role that the void spaces play
1056 during non-steady state permeation is not well understood. The results from
1057 our simulations of permeation with a reaction-diffusion representation of the
1058 dual mode model indicate that several hypotheses for the behavior of the
1059 void spaces during pre-steady state are reasonable, so long as the overall
1060 polymer response is delayed from the upstream pressure rise, as was also
1061 observed with the single mode model.

1062 The nanoscopic features of sorption and diffusion in polymers can be
1063 investigated directly with MD. In MD for glassy polymers, gas molecules are
1064 observed to occupy both void spaces and sites in which the polymer chains
1065 form a full coordination shell; these two types of sites are typically assumed
1066 to correspond to the Langmuir and dissolved sites, respectively, in the
1067 macroscopic dual mode description.⁹⁵ The void spaces obey a Poisson
1068 distribution with a high probability of finding very small voids and reduced
1069 probability of finding increasingly larger voids.³⁸ This is in contrast to the
1070 distribution implicitly assumed in the dual mode model, in which all void
1071 spaces are identical.³⁸ MD simulations of gas sorption in which the polymer
1072 structure is held static predict sorption isotherms that resemble classical
1073 Langmuir sorption isotherms, but are inconsistent with those for glassy
1074 polymers.³⁸ Allowing polymer relaxation during sorption produces isotherms
1075 that are more consistent with experiment.^{38, 96} This polymer relaxation in the
1076 presence of CO₂ is associated with shifting the FVE distribution to larger
1077 sizes.³⁸ It is unclear if the shift in FVE distribution is the same polymer

1078 relaxation being invoked in this work; additional experimental data would be
1079 needed to prove this connection.

1080 MD investigations of gas transport through glassy polymers shows that
1081 when gas molecules occupy a void site, they explore the full surface area of
1082 the void, and the rate-limiting step for their forward motion is polymer chain
1083 fluctuation creating a channel between voids then closing off space behind
1084 the molecule.³⁵⁻³⁷ The same type of “jump” diffusion in which molecules hop
1085 between FVE is observed in rubbery polymers;³⁴ however, the channels in a
1086 glassy polymer are longer-lived, meaning that the gas must wait a longer
1087 time for a productive forward jump, though still only on the order of
1088 nanoseconds.³⁵⁻³⁶ The free energy barriers for these jumps are shown to
1089 depend on the gas-polymer interactions (Fig. 5), resulting in different
1090 diffusion coefficients for different molecules even though polymer segmental
1091 motion is the rate-limiting step in both cases.

1092 The permeation mechanism evaluated in the present study for N₂ and
1093 CO₂ through PPO over extended time scales is consistent with this
1094 nanoscopic physical picture. The pressure-dependence of the diffusion
1095 coefficients in Figure 3c reveals that anomalous diffusion, in which both
1096 penetrant concentration gradient and polymer environment play a role, is
1097 operant. The presence of sorbed gas causes a relaxation (Figure 10) whose
1098 response time is roughly independent of gas type and thus appears to be
1099 polymer-dependent. In addition, the pressure dependence of the

1100 phenomenological diffusion coefficients in Figure 3c signals a change in the
1101 polymer structure with increasing permeant concentration. This effect is
1102 much more pronounced for CO₂ than for N₂. From consideration of the
1103 literature,^{27-28, 33, 38} it is likely that this polymer relaxation is related to the
1104 creation of FFV, but the reported time scale for this process is too fast to be
1105 probed directly by our current set of studies. This suggests that slower
1106 processes may also be involved. It is unclear from this study if the difference
1107 in free energy barriers in Figure 5a is a result of changes in FFV, differences
1108 in intermolecular interaction energies, or a combination thereof. Our work
1109 adds weight to the argument that polymer relaxation governs transport in
1110 glassy polymers by showing that it is kinetically significant not only on the
1111 very short timescales accessed by MD, but is also a general feature of non-
1112 steady state permeation of PPO for both CO₂ and N₂. The present study also
1113 augments the physical picture presented by MD calculations by revealing the
1114 importance of a timescale for the overall polymer response of the order of a
1115 few seconds, and the significant influence of a changing polymer
1116 environment on the macroscopic diffusion coefficient.

1117 Alternative models to the dual mode model are available but have not
1118 yet been widely adopted in the interpretation of experimental data; these
1119 include the site distribution (SD) model,^{31, 39, 71} the non-equilibrium lattice
1120 fluid model (NELF) model,⁹⁷ and the unified dual mode model.³² Due to their
1121 more realistic picture of microscopic aspects of permeation through glassy
1122 polymers, these models provide additional descriptions of the gas-polymer

1123 system that could be useful for the interpretation of glassy polymer solubility
1124 and transport data at steady state. To fully understand the gas-polymer
1125 interactions under non-steady state conditions using these models, reaction-
1126 diffusion simulations like the ones presented in this paper will be required.

1127 Conclusions

1128 We report new gas permeation measurements for PPO by N_2 and CO_2
1129 that provide time-dependent downstream pressure data for both steady and
1130 non-steady state regimes. Multiscale modeling incorporating physically-
1131 based reaction-diffusion kinetics and explicit gas uptake can reproduce the
1132 experimental data at steady and non-steady state using either single or dual
1133 mode transport models. Molecular dynamics simulations were performed to
1134 gain information on gas sticking to the PPO surface and show a sticking
1135 probability for CO_2 of 13%. Gas entry into the polymer is facile, so
1136 permeation is governed by polymer kinetics, not sticking. The equilibration
1137 between pressure and concentration in the polymer is not instantaneous;
1138 this slower polymer response must be included in the permeation
1139 mechanism to capture the pre-steady state behavior properly. Our findings
1140 along with other literature indicate that the common microscopic
1141 interpretation of the dual mode model is not self-consistent and does not
1142 explain the time-dependent permeation data for PPO. Rather, a molecular-
1143 level understanding of the diffusion process will serve to connect polymer
1144 structure to permeability, and to isolate polymer relaxation effects from
1145 specific chemical interactions that also influence permeation.

1146

1147 ASSOCIATED CONTENT

1148 **Supporting Information.** A file containing supplementary information can
1149 be found at [link] containing the molecular metadynamics methods,
1150 additional details of the multiscale model implementation, methods for and
1151 effects of correction of sorption and permeation data for swelling, tables with
1152 all simulation inputs, plots of all permeation experimental data, literature
1153 data on permeability and solubility in PPO, analysis of the correlation of
1154 permeability with Tg and density, experimental permeability data with a
1155 linear fit, additional results of the molecular metadynamics simulations,
1156 additional single mode model results, and additional dual mode model
1157 results. Data used in this paper are available at [link].

1158 AUTHOR INFORMATION

1159 **Corresponding Author** * E-mail: fahoule@lbl.gov

1160 **Conflict of Interest Disclosure.** The authors declare no competing
1161 interests.

1162 **Author Contributions.** The initial plan for this study was conceived by MS
1163 and FH, and developed together with AW and WG. MT performed the
1164 experiments, and MS, DB, AM, NH, LW and BM performed the calculations. All
1165 authors contributed to the interpretation of the experimental, theoretical and
1166 multiscale modeling results and preparation of the manuscript. All authors
1167 have given approval to the final version of the manuscript.

1168 **Acknowledgements.** The authors are grateful to Dr. Daniel J. Miller (JCAP,
1169 LBNL) for helpful discussions on membrane polymer science, and to Dr.
1170 William D. Hinsberg (Columbia Hill Technical Consulting) for discussions on
1171 the use of Kinetiscope in this work.

1172 **Funding Sources.** This material is based upon work performed by the
1173 Joint Center for Artificial Photosynthesis, a DOE Energy Innovation Hub,
1174 supported through the Office of Science of the U.S. Department of Energy
1175 under Award Number DE-SC0004993. All experiments and multiscale
1176 modeling were performed in the Hub. M. T. thanks the National Science
1177 Foundation Graduate Research Fellowship under Grant No. DGE 1106400. D.
1178 B., N.H., B. M., and W. A. G. acknowledge funding from Bosch Energy
1179 Research Network Grant No 07.23.CS.15 for the MD simulation work. Bosch
1180 Energy Research had no involvement in decisions concerning data collection,
1181 data processing, writing, or article submission.

1182

1183 References

- 1184 1. Hallinan, D. T.; Elabd, Y. A., Diffusion and Sorption of Methanol and
1185 Water in Nafion Using Time-Resolved Fourier Transform Infrared-Attenuated
1186 Total Reflectance Spectroscopy. *Journal of Physical Chemistry B* **2007**, *111*
1187 (46), 13221-13230.
- 1188 2. Hallinan, D. T., Jr.; Elabd, Y. A., Sorption and Diffusion Selectivity.
1189 Kakaç, S.; Al, E., Eds. Springer: Dordrecht, 2008; pp 189-208.
- 1190 3. Beckingham, B. S.; Lynd, N. A.; Miller, D. J., Monitoring Multicomponent
1191 Transport using In Situ ATR FTIR Spectroscopy. *Journal of Membrane Science*
1192 **2018**, *550*, 348-356.
- 1193 4. DeLuca, N. W.; Elabd, Y. A., Polymer Electrolyte Membranes for the
1194 Direct Methanol Fuel Cell: A Review. *Journal of Polymer Science Part B:*
1195 *Polymer Physics* **2006**, *44*, 2201-2225.
- 1196 5. Lewis, N. S.; Nocera, D. G., Powering the Planet: Chemical Challenges
1197 in Solar Energy Utilization. *Proceedings of the National Academy of Sciences*
1198 **2006**, *103* (43), 15729 LP-15735.
- 1199 6. Crank, J.; Park, G. S., *Diffusion in Polymers*. Academic Press Inc., Ltd.:
1200 London and New York, 1968.
- 1201 7. Wijmans, J. G.; Baker, R. W., The Solution-Diffusion Model: a Review.
1202 *Journal of Membrane Science* **1995**, *107*, 1-21.
- 1203 8. Petropoulos, J.; Sanopoulou, M.; Papadokostaki, K., Beyond Fick: How
1204 Best to Deal with non-Fickian Behavior in a Fickian Spirit. *Diffusion*
1205 *Fundamentals* **2009**, *11* (5), 1-21.
- 1206 9. Majsztrik, P. W.; Satterfield, M. B.; Bocarsly, A. B.; Benziger, J. B., Water
1207 Sorption, Desorption and Transport in Nafion Membranes. *Journal of*
1208 *Membrane Science* **2007**, *301* (1-2), 93-106.
- 1209 10. Daly, K. B.; Benziger, J. B.; Panagiotopoulos, A. Z.; Debenedetti, P. G.,
1210 Molecular Dynamics Simulations of Water Permeation across Nafion
1211 Membrane Interfaces. *Journal of Physical Chemistry B* **2014**, *118*, 8798-
1212 8807.
- 1213 11. Soniat, M.; Houle, F. A., Swelling and Diffusion during Methanol
1214 Sorption into Hydrated Nafion. *The Journal of Physical Chemistry B* **2018**,
1215 *122* (34), 8255-8268.
- 1216 12. Soniat, M.; Tesfaye, M.; Brooks, D.; Merinov, B.; Goddard lii, W. A.;
1217 Weber, A. Z.; Houle, F. A., Predictive Simulation of Non-Steady-State
1218 Transport of Gases Through Rubbery Polymer Membranes. *Polymer* **2018**,
1219 *134*, 125-142.
- 1220 13. Ghosal, K.; Freeman, B. D., Gas Separation Using Polymer Membranes:
1221 An Overview. *Polymers for Advanced Technologies* **1994**, *5* (11), 673-697.
- 1222 14. White, R. P.; Lipson, J. E. G., Polymer Free Volume and Its Connection
1223 to the Glass Transition. *Macromolecules* **2016**, *49* (11), 3987-4007.
- 1224 15. Shi, T.; Jiang, W.; An, L.; Li, B., Molecular Dynamics Simulation of Sub-
1225 Transition for Polyethersulfone. *Macromolecular Theory and Simulations*
1226 **2001**, *10* (4), 232-236.

- 1227 16. Yampolskii, Y. P.; Pinnau, I.; Freeman, B. D., *Materials Science of*
1228 *Membranes for Gas and Vapor Separation*. John Wiley & Sons Ltd: West
1229 Sussex, England, 2006; p 445-445.
- 1230 17. Sodaye, H. S.; Pujari, P. K.; Goswami, A.; Manohar, S. B., Probing the
1231 Microstructure of Nafion-117 Using Positron Annihilation Spectroscopy.
1232 *Journal of Polymer Science, Part B: Polymer Physics* **1997**, 35 (5), 771-776.
- 1233 18. Goworek, T. Positronium as a Probe of Small Free Volumes in Crystals,
1234 Polymers and Porous Media. 2014.
- 1235 19. Vrentas, J. S.; Vrentas, C. M., Sorption in Glassy Polymers.
1236 *Macromolecules* **1991**, 24, 2404-12.
- 1237 20. Maeda, Y.; Paul, D. R., Effect of Antiplasticization on Gas Sorption and
1238 Transport. II. Poly(phenylene Oxide). *Journal of Polymer Science: Part B:*
1239 *Polymer Physics* **1987**, 25, 981-1003.
- 1240 21. Bohlen, J.; Kirchheim, R., Macroscopic Volume Changes Versus
1241 Changes of Free Volume as Determined by Positron Annihilation
1242 Spectroscopy for Polycarbonate and Polystyrene. *Macromolecules* **2001**, 34
1243 (12), 4210-4215.
- 1244 22. Petropoulos, J. H., Quantitative analysis of gaseous diffusion in glassy
1245 polymers. *Journal of Polymer Science Part A-2: Polymer Physics* **1970**, 8 (10),
1246 1797-1801.
- 1247 23. Paul, D. R.; Koros, W. J., Effect of Partially Immobilizing Sorption on
1248 Permeability and the Diffusion Time Lag. *Journal of Polymer Science* **1976**,
1249 14, 675-685.
- 1250 24. Chern, R. T.; Sheu, F. R.; Jia, L.; Stannett, V. T.; Hopfenberg, H. B.,
1251 Transport of Gases in Unmodified and Aryl-Brominated 2,6-Dimethyl-1,4-
1252 Poly(Phenylene Oxide). *Journal of Membrane Science* **1987**, 35, 103-115.
- 1253 25. Bondar, V. I.; Kamiya, Y.; Yampol'skii, Y. P., On Pressure Dependence of
1254 the Parameters of the Dual-Mode Sorption Model. *Journal of Polymer Science,*
1255 *Part B: Polymer Physics* **1996**, 34 (2), 369-378.
- 1256 26. Kanehashi, S.; Nagai, K., Analysis of Dual-Mode Model Parameters for
1257 Gas Sorption in Glassy Polymers. *Journal of Membrane Science* **2005**, 253 (1-
1258 2), 117-138.
- 1259 27. Lo, C. H.; Hung, W. S.; De Guzman, M.; Huang, S. H.; Li, C. L.; Hu, C. C.;
1260 Jean, Y. C.; Lee, K. R.; Lai, J. Y., Investigation on CO₂-Induced Plasticization in
1261 Polycarbonate Membrane Using Positron Annihilation Lifetime Spectroscopy.
1262 *Journal of Membrane Science* **2010**, 363 (1-2), 302-308.
- 1263 28. Yuan, J.; Cao, H.; Hellmuth, E. W.; Jean, Y. C., Subnanometer Hole
1264 Properties of CO₂-Exposed Polysulfone Studied by Positron Annihilation
1265 Lifetime Spectroscopy. *Journal of Polymer Science Part B* **1998**, 36, 3049-
1266 3056.
- 1267 29. Aitken, C. L.; Koros, W. J.; Paul, D. R., Effect of Structural Symmetry on
1268 Gas Transport Properties of Polysulfones. *Macromolecules* **1992**, 25 (13),
1269 3424-3434.
- 1270 30. Böhning, M.; Springer, J., Sorptive Dilatation and Relaxational Processes
1271 in Glassy Polymer/Gas Systems-I. Poly(Sulfone) and Poly(Ether Sulfone).
1272 *Polymer* **1998**, 39 (21), 5183-5195.

- 1273 31. Kirchheim, R., Sorption and Partial Molar Volume of Small Molecules in
1274 Glassy Polymers. *Macromolecules* **1992**, 25 (25), 6952-6960.
- 1275 32. Guo, J.; Barbari, T. A., Unified Dual Mode Description of Small Molecule
1276 Sorption and Desorption Kinetics in a Glassy Polymer. *Macromolecules* **2009**,
1277 42 (15), 5700-5708.
- 1278 33. Houde, A. Y.; Kulkarni, S. S.; Kulkarni, M. G., Permeation and
1279 Plasticization Behavior of Glassy Polymers: A WAXD Interpretation. *Journal of*
1280 *Membrane Science* **1992**, 71 (1-2), 117-128.
- 1281 34. Fried, J. R.; Sadat-Akhavi, M.; Mark, J. E., Molecular Simulation of Gas
1282 Permeability: Poly(2,6-Dimethyl-1,4-Phenylene Oxide). *Journal of Membrane*
1283 *Science* **1998**, 149 (1), 115-126.
- 1284 35. Hofmann, D.; Fritz, L.; Ulbrich, J.; Paul, D., Molecular Simulation of
1285 Small Molecule Diffusion and Solution in Dense Amorphous Polysiloxanes and
1286 Polyimides. *Computational and Theoretical Polymer Science* **2000**, 10 (5),
1287 419-436.
- 1288 36. Hofmann, D.; Fritz, L.; Ulbrich, J.; Schepers, C.; Böhning, M., Detailed-
1289 Atomistic Molecular Modeling of Small Molecule Diffusion and Solution
1290 Processes in Polymeric Membrane Materials. *Macromolecular Theory and*
1291 *Simulations* **2000**, 9 (6), 293-327.
- 1292 37. Hofmann, D.; Heuchel, M.; Yampolskii, Y.; Khotimskii, V.; Shantarovich,
1293 V., Free Volume Distributions in Ultrahigh and Lower Free Volume Polymers:
1294 Comparison Between Molecular Modeling and Positron Lifetime Studies.
1295 *Macromolecules* **2002**, 35 (6), 2129-2140.
- 1296 38. Hölck, O.; Siegert, M. R.; Heuchel, M.; Böhning, M., CO₂ Sorption
1297 Induced Dilation in Polysulfone: Comparative Analysis of Experimental and
1298 Molecular Modeling Results. *Macromolecules* **2006**, 39 (26), 9590-9604.
- 1299 39. Neyertz, S.; Brown, D., Molecular Dynamics Study of Carbon Dioxide
1300 Sorption and Plasticization at the Interface of a Glassy Polymer Membrane.
1301 *Macromolecules* **2013**, 46 (6), 2433-2449.
- 1302 40. Neyertz, S.; Brown, D., The Effect of Structural Isomerism on Carbon
1303 Dioxide Sorption and Plasticization at the Interface of a Glassy Polymer
1304 Membrane. *Journal of Membrane Science* **2014**, 460, 213-228.
- 1305 41. Toi, K.; Morel, G.; Paul, D. R., Gas Sorption and Transport in
1306 Poly(phenylene Oxide) and Comparisons with Other Glassy Polymers. *Journal*
1307 *of Applied Polymer Science* **1982**, 27, 2997-3005.
- 1308 42. Bondi, A., *Physical Properties of Molecular Crystals, Liquids and*
1309 *Glasses*. Wiley: New York, 1968.
- 1310 43. Huang, Y.; Wang, X.; Paul, D. R., Physical Aging of Thin Glassy Polymer
1311 Films: Free Volume Interpretation. *Journal of Membrane Science* **2006**, 277
1312 (1-2), 219-229.
- 1313 44. *CRC Handbook of Chemistry and Physics: A Ready-Reference Book of*
1314 *Chemical and Physical Data*.
- 1315 45. *Springer Handbook of Materials Measurement Methods*. Springer:
1316 Berlin, 2006; p 1207.

1317 46. Wright, C. T.; Paul, D. R., Gas Sorption and Transport in UV-Irradiated
1318 Poly(2,6-dimethyl-1,4-phenylene oxide) Films. *Journal of Applied Polymer*
1319 *Science* **1998**, *67*, 875-883.

1320 47. Shin, H.; Pascal, T. A.; Goddard, W. A.; Kim, H., Scaled Effective Solvent
1321 Method for Predicting the Equilibrium Ensemble of Structures with Analysis of
1322 Thermodynamic Properties of Amorphous Polyethylene Glycol-Water
1323 Mixtures. *Journal of Physical Chemistry B* **2013**, *117* (3), 916-927.

1324 48. Plimpton, S., Fast Parallel Algorithms for Short-Range Molecular
1325 Dynamics. *Journal of Computational Physics* **1995**, *117*, 1-19.

1326 49. Banks, J. L.; Beard, H. S.; Cao, Y.; Cho, A. E.; Damm, W.; Farid, R.; Felts,
1327 A. K.; Halgren, T. A.; Mainz, D. T.; Maple, J. R.; Murphy, R.; Philipp, D. M.;
1328 Repasky, M. P.; Zhang, L. Y.; Berne, B. J.; Friesner, R. A.; Gallicchio, E.; Levy,
1329 R. M., Integrated Modeling Program, Applied Chemical Theory (IMPACT).
1330 *Journal of Computational Chemistry* **2005**, *26* (16), 1752-1780.

1331 50. Willard, A. P.; Chandler, D., Instantaneous Liquid Interfaces. *Journal of*
1332 *Physical Chemistry B* **2010**, *114* (5), 1954-1958.

1333 51. Julin, J.; Shiraiwa, M.; Miles, R. E. H.; Reid, J. P.; Pöschl, U.; Riipinen, I.,
1334 Mass Accommodation of Water: Bridging the Gap Between Molecular
1335 Dynamics Simulations and Kinetic Condensation Models. *Journal of Physical*
1336 *Chemistry A* **2013**, *117* (2), 410-420.

1337 52. Julin, J.; Winkler, P. M.; Donahue, N. M.; Wagner, P. E.; Riipinen, I., Near-
1338 Unity Mass Accommodation Coefficient of Organic Molecules of Varying
1339 Structure. *Environmental Science & Technology* **2014**, *48*, 12083-12089.

1340 53. Bowers, K.; Chow, E.; Xu, H.; Dror, R.; Eastwood, M.; Gregersen, B.;
1341 Klepeis, J.; Kolossvary, I.; Moraes, M.; Sacerdoti, F.; Salmon, J.; Shan, Y.;
1342 Shaw, D., Scalable Algorithms for Molecular Dynamics Simulations on
1343 Commodity Clusters. *ACM/IEEE SC 2006 Conference (SC'06)* **2006**,
1344 (November), 43-43.

1345 54. Shivakumar, D.; Williams, J.; Wu, Y.; Damm, W.; Shelley, J.; Sherman,
1346 W., Prediction of Absolute Solvation Free Energies using Molecular Dynamics
1347 Free Energy Perturbation and the OPLS Force Field. *Journal of Chemical*
1348 *Theory and Computation* **2010**, *6*, 1509-1519.

1349 55. Guo, Z.; Mohanty, U.; Noehre, J.; Sawyer, T. K.; Sherman, W.; Krilov, G.,
1350 Probing the α -Helical Structural Stability of Stapled p53 Peptides: Molecular
1351 Dynamics Simulations and Analysis. *Chem. Biol. Drug Des.* **2010**, *75*, 348-
1352 359.

1353 56. Bussi, G.; Donadio, D.; Parrinello, M., Canonical Sampling through
1354 Velocity Rescaling. *Journal of Chemical Physics* **2007**, *126* (1), 014101.

1355 57. Essmann, U.; Perera, L.; Berkowitz, M. L.; Darden, T.; Lee, H.; Pedersen,
1356 L. G., A Smooth Particle Mesh Ewald Method. *Journal of Chemical Physics*
1357 **1995**, *103* (19), 8577-8593.

1358 58. Pronk, S.; Páll, S.; Schulz, R.; Larsson, P.; Bjelkmar, P.; Apostolov, R.;
1359 Shirts, M. R.; Smith, J. C.; Kasson, P. M.; Van Der Spoel, D., GROMACS 4.5: A
1360 High-Throughput and Highly Parallel Open Source Molecular Simulation
1361 Toolkit. *Bioinformatics* **2013**, *29* (7), 845-854.

1362 59. Abraham, M. J.; Murtola, T.; Schulz, R.; Páll, S.; Smith, J. C.; Hess, B.;
1363 Lindahl, E., GROMACS: High Performance Molecular Simulations through
1364 Multi-Level Parallelism from Laptops to Supercomputers. *SoftwareX* **2015**, *1*,
1365 19-25.

1366 60. Tribello, G. A.; Bonomi, M.; Branduardi, D.; Camilloni, C.; Bussi, G.,
1367 PLUMED 2: New Feathers for an Old Bird. *Computational Physical*
1368 *Communications* **2014**, *185* (2), 604-613.

1369 61. Hess, B., P-LINCS: A Parallel Linear Constraint Solver for Molecular
1370 Simulation. *Journal of Chemical Theory and Computation* **2008**, *4* (1), 116-
1371 122.

1372 62. Bunker, D. L., Simple Kinetic Models from Arrhenius to the Computer.
1373 *Accounts of Chemical Research* **1974**, *7* (6), 195-201.

1374 63. Bunker, D. L.; Garrett, B.; Kleindienst, T.; Long, G. S., Discrete
1375 Simulation Methods in Combustion Kinetics. *Combustion and Flame* **1974**, *23*
1376 (3), 373-379.

1377 64. Gillespie, D. T., A General Method for Numerically Simulating the
1378 Stochastic Time Evolution of Coupled Chemical Reactions. *Journal of*
1379 *Computational Physics* **1976**, *22* (4), 403-434.

1380 65. Kinetiscope. <http://www.hinsberg.net/kinetiscope/>, 2017.

1381 66. Houle, F. a.; Hinsberg, W. D.; Morrison, M.; Sanchez, M. I.; Wallraff, G.;
1382 Larson, C.; Hoffnagle, J., Determination of Coupled Acid Catalysis-Diffusion
1383 Processes in a Positive-Tone Chemically Amplified Photoresist. *Journal of*
1384 *Vacuum Science & Technology B: Microelectronics and Nanometer Structures*
1385 **2000**, *18* (4), 1874-1874.

1386 67. Atkins, P.; de Paula, J., *Physical Chemistry*. 8th ed.; W. H. Freeman and
1387 Co.: New York, USA, 2006.

1388 68. Houston, P., *Chemical Kinetics and Reaction Dynamics*. DOVER
1389 PUBLICATIONS, INC.: Mineola, New York, 2001; p 48-49.

1390 69. Somorjai, G. A.; Li, Y., *Introduction to Surface Chemistry and Catalysis*.
1391 Wiley: 2010; p 800-800.

1392 70. Engel, T.; Reid, P., *Thermodynamics, Statistical Thermodynamics, &*
1393 *Kinetics*. 2nd ed.; Prentice Hall: 2010.

1394 71. Gotthardt, P.; Grüger, A.; Brion, H. G.; Plaetschke, R.; Kirchheim, R.,
1395 Volume Change of Glassy Polymers by Sorption of Small Molecules and its
1396 Relation to the Intermolecular Space. *Macromolecules* **1997**, *30* (25), 8058-
1397 8065.

1398 72. Story, B. J.; Koros, W. J., Sorption and Transport of CO₂ and CH₄ in
1399 Chemically Modified Poly(Phenylene Oxide). *Journal of Membrane Science*
1400 **1992**, *67* (2-3), 191-210.

1401 73. Aguilar-Vega, M.; Paul, D. R., Gas Transport Properties of
1402 Polyphenylene Ethers. *Journal of Polymer Science Part B: Polymer Physics*
1403 **1993**, *31* (11), 1577-1589.

1404 74. Huang, Y.; Paul, D. R., Effect of MolecularWeight and Temperature on
1405 Physical Aging of ThinGlassy Poly(2,6-dimethyl-1,4-phenylene oxide) Films.
1406 *Journal of Polymer Science Part B: Polymer physics* **2007**, *45* (April), 1390-
1407 1398.

1408 75. Tran, A.; Kruczek, B., Development and Characterization of
1409 Homopolymers and Copolymers from the Family of Polyphenylene Oxides.
1410 *Journal of Applied Polymer Science* **2007**, *106*, 2140-2148.

1411 76. Maeda, Y.; Paul, D. R., Effect of Antiplasticization on Gas Sorption. III.
1412 Free Volume Interpretation. *Journal of Polymer Science: Part B: Polymer*
1413 *Physics* **1987**, *25*, 1005-1016.

1414 77. Assogna, A.; Perego, G.; Roggero, A.; Sisto, R.; Valentini, C., Structure
1415 and Gas Permeability of Silylated Poly(Phenylene Oxide). *Journal of*
1416 *Membrane Science* **1992**, *71*, 97-103.

1417 78. Jian, Z.; Xiaohuai, H., The Gas Permeation Property in Trimethylsilyl-
1418 Substituted PPO and Triphenylsilyl-Substituted PPO. *Journal of Membrane*
1419 *Science* **1994**, *97*, 275-282.

1420 79. Alentiev, A.; Drioli, E.; Gokzhaev, M.; Golemme, G.; Ilinich, O.; Lapkin,
1421 A.; Volkov, V.; Yampolskii, Y., Gas Permeation Properties of Phenylene Oxide
1422 Polymers. *Journal of Membrane Science* **1998**, *138* (1), 99-107.

1423 80. *Polymer Data Handbook*. Oxford University Press: 1999; p 1264-1264.

1424 81. Kolb, C. E.; Cox, R. A.; Abbatt, J. P. D.; Ammann, M.; Davis, E. J.;
1425 Donaldson, D. J.; Garrett, B. C.; George, C.; Griffiths, P. T.; Hanson, D. R.;
1426 Kulmala, M.; McFiggans, G.; Pöschl, U.; Riipinen, I.; Rossi, M. J.; Rudich, Y.;
1427 Wagner, P. E.; Winkler, P. M.; Worsnop, D. R.; O'Dowd, C. D., An overview of
1428 current issues in the uptake of atmospheric trace gases by aerosols and
1429 clouds. *Atmospheric Chemistry and Physics* **2010**, *10* (21), 10561-10605.

1430 82. Lancaster, D. K.; Johnson, A. M.; Burden, D. K.; Wiens, J. P.; Nathanson,
1431 G. M., Inert gas scattering from liquid hydrocarbon microjets. *Journal of*
1432 *Physical Chemistry Letters* **2013**, *4* (18), 3045-3049.

1433 83. Lu, J. W.; Morris, J. R., Gas-Surface Scattering Dynamics of CO₂, NO₂,
1434 and O₃ in Collisions with Model Organic Surfaces. *Journal of Physical*
1435 *Chemistry A* **2011**, *115*, 6194-6201.

1436 84. Alexander, W. a.; Zhang, J.; Murray, V. J.; Nathanson, G. M.; Minton, T.
1437 K., Kinematics and Dynamics of Atomic-Beam Scattering on Liquid and Self-
1438 Assembled Monolayer Surfaces. *Faraday Discussions* **2012**, *157*, 355-374.

1439 85. Donaldson, D. J., Adsorption of Atmospheric Gases at the Air–Water
1440 Interface. I. NH₃. *Journal of Physical Chemistry A* **1999**, *103* (1), 62-70.

1441 86. COMSOL Multiphysics® v. 5.4. COMSOL AB, Stockholm, Sweden.
1442 www.comsol.com.

1443 87. Chandler, D., *Introduction to Modern Statistical Mechanics*. Oxford
1444 University Press: Oxford, 1987; p 274.

1445 88. Minelli, M.; Sarti, G. C., Permeability and Solubility of Carbon Dioxide in
1446 Different Glassy Polymer Systems with and without Plasticization. *Journal of*
1447 *Membrane Science* **2013**, *444*, 429-439.

1448 89. Minelli, M.; Sarti, G. C., Gas transport in glassy polymers: Prediction of
1449 diffusional time lag. *Membranes* **2018**, *8* (1), 1-15.

1450 90. Koros, W. J.; Chan, A. H.; Paul, D. R., Sorption and Transport of Various
1451 Gases in Polycarbonate. *Journal of Membrane Science* **1977**, *2*, 165-190.

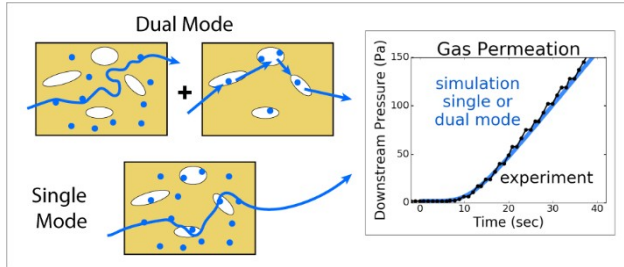
- 1452 91. McHattie, J. S.; Koros, W. J.; Paul, D. R., Effect of Isopropylidene
1453 Replacement on Gas Transport Properties of Polycarbonates. *Journal of*
1454 *Polymer Science: Part B Polymer Physics* **1991**, 29, 731-746.
- 1455 92. Aitken, C. L.; Koros, W. J.; Paul, D. R., Gas Transport Properties of
1456 Biphenol Polysulfones. *Macromolecules* **1992**, 25, 3651-3658.
- 1457 93. Erb, A. J.; Paul, D. R. *Gas Sorption and Transport in Polysulfone*; 1981;
1458 pp 11-22.
- 1459 94. Breck, D. W., *Zeolite molecular sieves: structure, chemistry, and use*.
1460 R.E. Krieger: 1984.
- 1461 95. Neyertz, S.; Brown, D., Oxygen Sorption in Glassy Polymers Studied at
1462 the Molecular Level. *Macromolecules* **2009**, 42 (21), 8521-8533.
- 1463 96. Kupgan, G.; Demidov, A. G.; Colina, C. M., Plasticization behavior in
1464 polymers of intrinsic microporosity (PIM-1): A simulation study from
1465 combined Monte Carlo and molecular dynamics. *Journal of Membrane*
1466 *Science* **2018**, 565, 95-103.
- 1467 97. Doghieri, F.; Sarti, G. C., Nonequilibrium Lattice Fluids: A Predictive
1468 Model for the Solubility in Glassy Polymers. *Macromolecules* **1996**, 29 (24),
1469 7885-7896.

1470

1471

1472 Table of Contents Graphic

1473



1474